ONR-URI Composites Program
Technical Report No. 90-02

UIUC-NCCMR-90-02

BUCKLING AND POSTBUCKLING ANALYSES OF FIBER-COMPOSITE LAMINATE PLATES UNDER BIAXIAL COMPRESSION

Laurent Rouxel* and S.S. Wang**

January, 1990

National Center for Composite Materials Research
at University of Illinois, Urbana - Champaign
A DoD University Research Initiatives Center funded by the
Office of Naval Research, Arlington, VA

* Research Assistant

** Professor and Director

ABSTRACT

Developments of advanced fiber-composite laminates as viable structural components have introduced new complexities in design. Among these concerns is the load-bearing capacity of these structures under multiaxial compressive loading. In this study deformations and transverse shear stresses at buckling and in the postbuckling range are analyzed to study the compressive failure behavior of thin- and thick-section composite laminates.

The general formulation for buckling and postbuckling is based on Newton/Raphson and Riks algorithms used in conjunction with a nonlinear large deformation finite-element method. In order to assess the effect of transverse shear on the buckling and postbuckling behavior a deformable shear plate formulation is used.

The global load-deformation response and the transverse shear development in the composite laminates during buckling and postbuckling are studied. Potential changes in buckling mode in postbuckling are especially considered. Effects of thickness, imperfection sensitivity, stress-biaxiality ratio, boundary conditions and lamination layup on global buckling and postbuckling response and on transverse shear development are also analyzed.

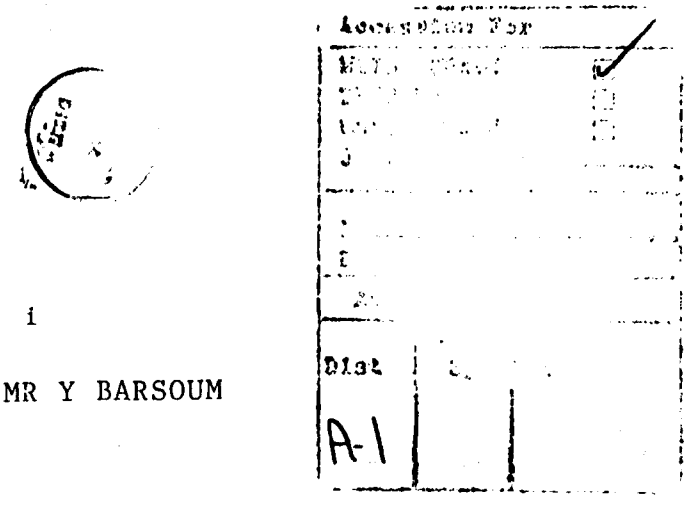

TABLE OF CONTENTS

LIST OF FIGURE CAPTIONS

1. INTRODUCTION

Composite materials offer attractive potentials to be tailored for advanced engineering applications, for example high specific strength, specific stiffness and fatigue resistance. With rapid developments of advanced fiber composites as viable structural materials, evaluation, analysis and prediction of the material behavior and structural performance with various lamination variables and geometric configurations have become a primary concern, especially under compression. However, along with improved structural performance provided by composite materials, it has also come a level of complexity much greater than that encountered in conventional monolithic materials. Additional complexities are related to material anisotropy and heterogeneity, material and structural discontinuities and the large number of lamination parameters involved. Especially high-performance thick-section composite structures developing highly tridimensional stress fields are prevalent.

A considerable amount of literature has been available, in both analytical and experimental studies, which adresses the problem of orthotropic plates under uniaxial compressive loading. Studies on the behavior of composite plates under general biaxial compressive loading has not been comprehensive. The effect of the interlaminar stresses on buckling and postbuckling behavior of the composite laminates has not been fully studied yet. These stresses are expected to have a negative effect on these structures, by reducing the corresponding structure stiffness as well as inducing failure through delamination. Properly understanding the development of transverse shear

stresses in the postbuckling range will enable us to assess qualitatively and quantitatively their local and global effects on the structure response. These studies have a higher degree of complexity because of the non-linear geometric and material considerations involved. A brief literature review on the buckling and postbuckling analyses of fiber-composite plates is given in the next section.

Current design philosophy is directed to require these composite components to carry the load well into the postbuckling state. Thus the buckling and postbuckling behavior of fiber-composite laminates under various combinations of biaxial compression should be carefully studied. The large number of problem parameters involved, such as geometry, constituent materials, lamination, boundary conditions and load characteristics, should be analyzed systematically to provide a comprehensive understanding of the compressive instability problem.

In this study, a detailed analysis of the mechanical response of composite structures under biaxial compressive loading is conducted. These analyses are carried out by the use of a nonlinear finite element method as discussed in Sec. 3. Buckling and postbuckling deformations and associated characteristics of fiber-composite laminated plates have been obtained. Magnitudes and effects of transverse shear stresses, which arise especially in the postbuckling range for thick laminates, are determined in Sec. 4. Also, effects of boundary conditions, lamination stacking sequence and stress-biaxiality ratio on the buckling and postbuckling behavior are examined.

2. LITERATURE REVIEW

2.1. BUCKLING ANALYSES OF COMPOSITE LAMINATES

Approximate analytical solutions for predicting buckling loads of composite laminates, based on Galerkin and Rayleigh-Ritz methods, have been reported by many researchers [1-3]. For example, Ashton and Love [2] have used the Rayleigh-Ritz method in the case of anisotropic thin plates under shear stress. Experiments have also been conducted and good agreement between experimental and analytical results has been obtained.

The effect of transverse shear deformation through composite plate thickness, especially in thick composites, on buckling has been studied by several researchers [3-4], using Mindlin-type plate formulation in an analytical approach or a finite-element approach. These studies depict the decreasing effect of transverse shear deformation on the buckling load. This effect has been shown to be more important for the cases with clamped boundary conditions than with simply-supported ones.

Limitations of the Mindlin-type, plate formulation to model the behavior of thick composite laminates motivate the development of buckling analyses, using higher-order plate formulations or a 3-D approach in conjunction with the finite element method. The 3-D displacement-based, element, developed by Owen and Li [5], makes use of piecewise linear approximations for in-plane displacements and a constant transverse displacement through the element thickness, and in-plane quadratic interpolation for these three displacement

variables. A linearized buckling analysis has been developed and more accurate results than conventional thin and thick composite plate formulations have been obtained for modelling the negative effect of transverse shear deformation. It also offers simplicity and computer-time economy when used in conjunction with a substructuring technique, compared to a hybrid-stress, 3-D multilayer finite-element formulation [6]. However the 3-D displacement-based, finite-element formulation may not accurately model the 3-D stress state in composite laminates since conditions of interface continuity of interlaminar stresses, and surface traction-free boundary conditions at the edges and other geometric boundaries are satisfied only approximately.

The hybrid-stress finite-element formulation originally developed by Pian [6] overcomes these limitations. Interlaminar stress continuity at layer interfaces and surface traction-free boundary conditions are exactly satisfied through the assumption of an equilibrium stress field by introducing proper lamina stress parameters. But formulation is generally rather elaborate and complex, and may require a large amount of computing time so that its use is still limited to advanced researchers. No analysis of buckling of composite laminates has been conducted using this formulation.

2.2. POSTBUCKLING ANALYSES OF COMPOSITE PLATES

Postbuckling responses of thick composite laminates in shear and under biaxial compression have been obtained by various methods, for example, the Rayleigh-Ritz method [7] and the finite element method [8]. Both Kirchhoff thin-plate and Mindlin plate formulations have been considered. The results show that

transverse shear reduces the postbuckling stiffness of a thick composite laminate plate for both loading cases considered. Moreover, results from [8] has pointed out the drastic effect of boundary conditions on the buckling load and postbuckling stiffness of composite structures.

Only few comparisons between analytical results and experimental data of buckling and postbuckling of fiber-composite laminates have been conducted. Numerical solutions, using finite element methods [9] and the Rayleigh-Ritz energy method [10], have been shown to correlate well with the experimental behavior of thin composite laminate plates with unidirectional, quasi-isotropic and general fiber orientations under uniaxial compression up to failure. However, no comparison has been made for thick laminates or fiber composites subjected to biaxial compression. Therefore accuracy of the numerical solutions based on transverse-shear deformation theories or 3-D solid element formulation to evaluate the effect of interlaminar stresses on the postbuckling response of thick laminates has not been validated.

3. METHODS OF ANALYSIS

At buckling, bifurcation from the primary in-plane deformation state to an out-of-plane deformation state occurs. At the critical point, variation of the potential energy is zero (neutral equilibrium) which leads to the bending strain energy equal to the external work done by the in-plane loads. During postbuckling, the out-of-plane deformation becomes stable and the corresponding potential energy of the structure is minimum. Therefore the structure deforms in this secondary deformation state with increasing in-plane compressive load.

This study makes use of the finite element method implemented in ABAQUS finite element program [11]. Versatility and applicability of this method enable to model accurately the buckling and postbuckling of composite structures with critical responses, such as changes in buckling mode, presence of a cutout or highly tridimensional stress field. The latter two cases will be especially investigated in future studies.

3.1. FINITE ELEMENT FORMULATION

The finite element procedure used in ABAQUS is based on the incremental, updated Lagrangian formulation. This formulation expresses equilibrium at a particular load level in terms of the previously calculated equilibrium configuration. At the end of every increment, the coordinates of the body are updated using the incremental displacements predicted. The principle of virtual work is generally used for this formulation. By using the finite

element modeling scheme for spatial discretization, a system of non-linear algebraic equations results in the form:

$$\underset{\sim}{K}_t \, \Delta\underset{\sim}{U} = \Delta\underset{\sim}{P} \tag{1}$$

with:
- $\underset{\sim}{K}_t$ tangent stiffness matrix
- $\Delta\underset{\sim}{U}$ incremental nodal displacement vector
- $\Delta\underset{\sim}{P}$ incremental nodal force vector

3.1.1. Linearized buckling analysis

Assuming that the deformation is linear before buckling with small deformations, the terms which are functions of nodal displacements in the general non-linear tangent stiffness matrix can be neglected. The linearized formulation then gives rise to a tangent stiffness matrix with the following expression:

$$\underset{\sim}{K}_t = \underset{\sim}{K}_L + \underset{\sim}{K}_g(\sigma) \tag{2}$$

where $\underset{\sim}{K}_L$ is a linear stiffness matrix and $\underset{\sim}{K}_g$ a geometric stiffness matrix linearly dependent upon the stresses.

The bifurcation solution for the linearized buckling problem may be determined from the following eigenvalue equation:

$$[\underset{\sim}{K}_L + \lambda \underset{\sim}{K}_g(\sigma_o)] \, \underset{\sim}{U} = \underset{\sim}{0} \tag{3}$$

where λ is an eigenvalue and $\underset{\sim}{U}$ an eigenvector. The critical load P_{cr} can be found from $P_{cr} = \lambda \, P_o$ where P_o is the nominal load which corresponds to the stress state σ_o.

A subspace iteration procedure is used in ABAQUS to solve for the eigenvalues and eigenvectors. The buckling load is then governed by the lowest eigenvalue, and the buckling mode by the corresponding eigenvector.

3.1.2. Postbuckling analysis

During postbuckling the nonlinear equilibrium equations (1) are solved at each load increment using the Newton-Raphson method. In order to model the potential decrease in the load and displacement as the solution evolves (case of unstable problems), a modified Riks nonlinear incremental-iterative algorithm [12] is used (implemented in ABAQUS) to construct the equilibrium solution path. In this modified Riks scheme, as in the basic Riks algorithm [13], the nonlinear procedure is based on a motion along the tangent line (defined by the tangent stiffness matrix) at the previous solution point of a given distance. Search for an equilibrium solution in the plane that passes through the point perpendicular to the same tangent line can be carried out using an iterative algorithm.

To model bifurcation from the prebuckling path to the postbuckling path, geometric imperfection, in the form of transverse displacements along the z-axis (see Fig. 1 for the plate geometry), is introduced in the nodal coordinates in the initial state. The imperfection is generally constructed from a linear combination of the three lowest eigenmodes of the structure, determined by a linearized buckling analysis, as follows:

$$\underset{\sim}{I} = \epsilon \, [\pm \underset{\sim}{M}_1 \pm \underset{\sim}{M}_2 \pm \underset{\sim}{M}_3] \tag{4}$$

where $\underset{\sim}{I}$ is the resulting imperfection, ϵ is a scaling coefficient, and $\underset{\sim}{M}_1$, $\underset{\sim}{M}_2$,

$\underset{\sim}{M}_3$ are the normalized eigenmodes.

3.1.3. Element formulation

The element used is a degenerated plate element from an isoparametric 8-nodes quadrilateral shell element with six degrees of freedom per node (three displacements and three rotations). This shell element is based on a shear-deformable shell formulation [14] which allows transverse shear deformation. This element formulation has been implemented in ABAQUS finite element program and is used in the analyses performed in this study.

From the analysis, values of transverse shear forces Q_x and Q_y at each Gaussian point of the element are determined in every load increment. These forces represent resultants of transverse shear stresses along the laminate thickness directions:

$$Q_x = \int_{-t/2}^{t/2} \tau_{xz}\, dz \qquad\qquad Q_y = \int_{-t/2}^{t/2} \tau_{yz}\, dz \tag{5}$$

Therefore they give a first insight in the effect of transverse shear on buckling and postbuckling of fiber-composite plates.

3.2. Solution accuracy and convergence

Validity studies of the buckling and postbuckling finite-element formulations are conducted for a thin composite plate. Comparisons are made with experimental data and numerical results [9] for a rectangular carbon-epoxy composite plate with $[\pm 45/0_2/\pm 45/0_2/\pm 45/0/90]_s$ stacking sequences (Fig. 2).

As in the numerical solution of this Reference, the imperfection is taken as the lowest mode (buckling mode) scaled to 1% of the plate thickness. Mesh refinements are conducted. Buckling load and postbuckling stiffness of the present solutions obtained are in excellent agreement with the reference solution.

In addition to the aforementioned comparison, detailed studies of the buckling and postbuckling finite-element solutions are also carried out to ensure the convergence of global load/end shortening relationship and transverse shear developed in the postbuckling range, in composite laminates with different lamination and geometric parameters.

Three mesh refinements are first conducted to examine the composite load/displacement response. The three composite plates considered here have clamped boundary conditions on all sides but differ in lamination and geometric parameters. For the first case the plate considered is a 0^{o} unidirectional laminated plate under biaxial compression ($N_x/N_y = 2$) with a thickness/length ratio of 0.05. For the two following cases quasi-isotropic laminate plates with $[0/90/\pm45]_{ns}$ stacking sequences under biaxial compression ($N_x/N_y = 2$) are studied for different thickness/length ratios. The second case corresponds to a ratio of 0.02 while the last one has a ratio of 0.08. These three composite plates are used in the analyses described in Sec. 4.

Solution convergence is found to depend strongly on the laminate thickness/length ratio. The larger this ratio is, the slower the rate of convergence obtained is. For the lowest ratio considered ($t/L = 0.02$) the

converged mesh is a 5x5 finite-element mesh (Fig. 3) while for increasing ratios (0.05 and 0.08) the converged meshes are a 6x6 finite-element mesh (Fig. 4) and a 9x9 finite-element mesh (Fig. 5), respectively. The highest ratio gives a much smaller rate of convergence because activation of higher (i.e. second and third) modes takes place in the postbuckling range beyond $N_x = 1.5\ N_{xcr}$ (Fig. 5). No change in buckling mode really occurs as the structure gradually losses its stiffness and becomes unstable. Corresponding loss of stability of the numerical solution are obtained at decreasing load levels for increasing mesh refinements.

Convergence of transverse shear stress solutions developed in the postbuckling range is also studied. The case considered is a clamped laminated plate with $[0/90/\pm45]_{12s}$ layup under biaxial compression ($N_x/N_y = 2$) with a thickness/length ratio of 0.04 corresponding to the analyses performed in Sec. 4.2. Two types of convergence parameters are selected: the transverse force distributions over the whole structure and the local transverse section forces at the particular location (x,y) = (-3,-3) (in) (see Fig. 1 for the plate geometry). In this last case the forces are interpolated from the values of transverse section forces at the four Gaussian points of the element containing this location (using a bilinear interpolation).

As expected, the rate of convergence for the transverse shear stress solutions is much smaller than the one for the global load/end shortening response, since transverse shear stresses are rather local. For the case with 25 elements (5x5 mesh) the finite element model gives a converged result for the load/end shortening curve (Fig 6). On the other hand, 81 elements (9x9 mesh)

are needed to get accurate transverse forces. For the transverse shear stresses at the specific location as previously defined, an 81-element mesh gives a good convergence too (Figs. 7-8).

4. ANALYSES AND RESULTS

The composites studied are fiber-composite laminate plates (Fig. 1) made of AS4 fibers and a J1 thermoplastic-matrix material. The plates have a square geometry with a constant lamina thickness of 0.005 (in). Biaxial in-plane loading is applied in the form of uniform displacements along the edges of the laminates. Two plate geometries with specific laminate characteristics are analyzed.

In Sec. 4.1.3. and part of Sec. 4.1.1., a unidirectional laminate (in the X-direction) with dimensions fixed to L = 8 (in), t = 0.40 (in) is considered. The elastic properties of the AS4/J1 composite material in tension are: E_{11} = 17.9 x 10^6 (psi), E_{22} = 0.9 x 10^6 (psi), ν_{12} = 0.313, G_{12} = G_{13} = 0.77 x 10^6 (psi), G_{23} = 0.31 x 10^6 (psi)

In other analyses, the lengths of the laminated square plates studied are 12 (in) in either directions and the compressive moduli of the AS4/J1 composite material are used. This changes E_{11} to 15.6 x 10^6 (psi) while other elastic properties remain the same. Laminate thickness and lamination parameters may be different in each case and will be defined in the corresponding sections.

Finite-element models of the full composite plate are used in all analyses. These enable to predict general buckling mode and higher modes (symmetric and antisymmetric) and corresponding critical loads in one linearized buckling analysis. Moreover, using these finite-element meshes combined with imperfections constructed from the three lowest eigenmodes, potential changes

in buckling mode can be modelled in the nonlinear buckling and postbuckling analysis. Solutions for the load/end shortening response are usually presented with respect to the normalized loading and displacement variables N_x/N_{xcr} and U/U_{cr}, respectively. N_{xcr} is taken as the buckling load given by a linearized buckling analysis, and U_{cr} as the corresponding critical end shortening on the load/displacement curve.

4.1. GLOBAL LOAD-DEFORMATION RESPONSE DURING BUCKLING AND POSTBUCKLING

4.1.1. Imperfection sensitivity

4.1.1.1. Buckling and postbuckling without change in buckling mode

The sensitivity of global buckling and postbuckling to the structural imperfection is studied. The finite element analyses make use of the 6x6 and 5x5 converged finite-element models, respectively, obtained in the mesh refinements performed previously. The imperfection sensitivity is shown to be more important for the first case (unidirectional laminate plate) (Fig. 9) than for the second case (quasi-isotropic laminate plate) (Fig. 10). The former gives a slightly higher postbuckling stiffness for the case with a 0.1% imperfection than those with 1% and 10% imperfections (with respect to the laminate thickness), while the latter gives the same postbuckling responses for the cases with 0.1% and 1% imperfections, and a very close one for the case with 10% imperfection. The imperfection sensitivity is likely to depend on the level of anisotropy of the laminate. However, since the geometric characteristics of the plates studied in both cases are different (especially

the width/thickness ratio), no rigorous conclusion can be made.

4.1.1.2. Buckling and postbuckling with change in buckling mode

For the analysis presented in Sec. 4.2.2. (quasi-isotropic clamped plate under uniaxial compression) a change in buckling mode is determined in the postbuckling range. The first deformation mode after buckling is made of one half sine-wave in both directions (i.e., the symmetric mode) while the new buckling mode after bifurcation is antisymmetric with two half sine-waves in the X-direction and one in the Y-direction (see Figs. 11-12). After the validity of the bifurcation analysis is established, the effect of the imperfection magnitude (ϵ) is studied. For small imperfections (e.g., ϵ = 0.1% and 1% of the plate thickness) a snap-back type behavior is obtained with similar postbuckling responses for both imperfection magnitudes considered. For a large imperfection (e.g., ϵ = 10% of the plate thickness) the change in the buckling mode occurs gradually at a low load level without snap-back response (Fig. 13). The out-of-plane displacements are noted to change differently with nominal loading for the cases with various imperfections (i.e., 1% and 10% of the plate thickness), (Figs. 14-15). The displacements are at locations (x,y) = ($\pm$2,0) (in) near the points of maximum deflection in the antisymmetric mode. According to Figs. (13-15) the load at which the change in buckling mode occurs can be determined as follows:

- For the case with 0.1% and 1% imperfections (Fig. 13) it is the maximum load before the snap-back response starts, which leads to a decrease in the in-plane loading (This corresponds to N_X = 1.47 N_{Xcr} for 0.1% imperfection.).

- For the case with 10% imperfection, it is the load at which a change in postbuckling stiffness occurs in the load/end shortening curve (Fig. 13). This load corresponds to a "plateau" for the transverse displacement at (x,y) = (-2,0) (in) and a zero value for the transverse displacement at (x,y) = (2,0) (in) (Fig. 15). This load value is $N_x = 1.16\ N_{xcr}$ in this case.

The load at which a change in buckling mode occurs depends on the imperfection magnitude used in the nonlinear buckling and postbuckling analysis, whereas imperfection does not affect the buckling load, as shown previously and in Fig. 13. In such analysis, the buckling load is defined as the first change in slope of the load/end shortening curve and corresponds precisely to the first eigenvalue λ_1 given by a linearized buckling analysis. On the other hand, higher eigenvalues (λ_2, λ_3, ...etc) calculated by this linearized buckling analysis can not represent accurately the loads at which actual changes in buckling modes may occur. Such an eigenvalue ($\lambda > \lambda_1$) is computed as the point of neutral equilibrium between its buckling mode (eigenmode) and the primary in-plane deformation mode (prior to buckling). However change in buckling mode actually appears after buckling at the point of neutral equilibrium between the new buckling mode (eigenmode of eigenvalue $\lambda > \lambda_1$) and the previous buckling mode (e.g., eigenmode of eigenvalue λ_1) .

Another concern is the sensitivity of composite buckling and postbuckling to the shape of the imperfections introduced. For the results presented previously, a specific linear combination of the three lowest eigenmodes gives imperfection shapes close to the first mode (Fig. 16). Using a different linear combination of the three lowest modes (i.e., changing signs of

normalized eigenmodes when adding them together, as defined in Eq. (4) Sec. 3.1.2.), another type of imperfection shape can been defined (Fig. 17). This second shape is close to the second mode of the structure. Therefore comparison between buckling and postbuckling solutions obtained with these two extreme imperfection shapes should clearly characterize the extent of the sensitivity of the structure to different imperfections.

For the case with 10% imperfection, the load/end shortening curves obtained with the two imperfection shapes are slightly different (Fig. 18). The solution corresponding to an imperfection shape close to the second eigenmode is slightly lower than the other one, and the change in buckling mode occurs much more gradually. In that case the activation of the second mode at buckling is more important since the imperfection shape is closer to the second mode. By examining the transverse displacement development for this imperfection, the composite plate is found to buckle in a mode made of its two lowest modes with the second mode gradually becoming the preponderant one. No sudden change in postbuckling stiffness occurs and no precise load for the change in buckling mode can be defined.

With a 1% imperfection, the postbuckling responses for both imperfection shapes are very similar (Fig. 19). Buckling occurs in the first mode of the structure, and the composite encounters a snap-back behavior when it changes in buckling mode. For these two extreme imperfection shapes, the only difference noticed in the postbuckling response is the load at which the snap-back response starts. The solution using the imperfection shape close to the second eigenmode gives a lower bifurcation load than the other one. Therefore

activation of this mode takes place sooner after buckling in that case.

These analyses show that buckling and postbuckling responses of a composite laminate plate are sensitive to imperfections in the case of a change in buckling mode only. Imperfection magnitude is more critical than imperfection shape in that case. In subsequent analyses of Sec. 4.1., the imperfections used have magnitudes equal to 1% of the laminate plate thickness and shapes close to the first eigenmode (buckling mode).

4.1.2. Effect of stress-biaxiality ratio

The composite plate studied is a $[0/90/\pm45]_{6s}$ clamped plate with a thickness/length ratio of 0.02. The values chosen for the stress-biaxiality ratio (N_x/N_y) are: 0, 0.25, 0.5, 1, 2, 4, 8 ,16 and ∞ (case of uniaxial compression along the X-axis). As expected, the buckling loads for N_x/N_y equal to 0 and ∞, 0.25 and 4, 0.5 and 2, respectively, are the same with interchanging N_{xcr} and N_{ycr}. A buckling envelope in the compression-compression range is constructed (Fig. 20) and is almost a straight line, the buckling modes in both directions being the same (one half sine-wave).

In the postbuckling range, higher levels of biaxial stress state compared to the uniaxial case are shown to reduce the postbuckling stiffness in both directions (Figs. 21-22), especially in the transverse direction (Y-axis). Fig. 22 shows also that for a low level of the biaxial stress state, buckling changes the sign of tangent stiffness which was negative in the prebuckling range. In these cases the state of deformation turns from tension to

compression in the Y-direction at buckling (positive postbuckling stiffness).

4.1.3. Effect of boundary conditions

Comparisons of four types of boundary conditions are performed for the case of a 0^{o} unidirectional laminate square plate (with a thickness/length ratio of 0.05) under uniaxial compression ($N_y = 0$) and biaxial compression ($N_x/N_y = 2$). The four boundary conditions are:

(1) All edges are clamped (clamped/clamped case)

(2) All edges are simply-supported (S.S./S.S. case)

(3) The edges perpendicular to the X-axis are simply-supported, and the edges perpendicular to the Y-axis, clamped (S.S./clamped case)

(4) The edges perpendicular to the X-axis are clamped, and the edges perpendicular to the Y-axis, simply-supported (clamped/S.S. case)

Figs. (23-24) show very interesting results. The full clamped plate does not necessarily give the highest postbuckling stiffness for both loading cases. Actually the clamped/S.S. case and the S.S./clamped case give, respectively, the lowest and highest stiffness in uniaxial compression, while in biaxial compression the fully simply-supported plate gives a much lower postbuckling stiffness than other cases. In terms of buckling load, the fully clamped plate has the highest buckling load, as expected, while the fully simply-supported plate has the lowest, in both loading conditions. The ratio of the buckling load for the clamped plate to the one for the simply-supported plate is 2.9 in uniaxial compression and 2.3 in biaxial compression.

These results (Figs. 23-24) demonstrate the important effects of boundary conditions on the buckling and postbuckling behavior and the interaction effects between boundary conditions and loading variables.

4.1.4. Effect of lamination layup

The composite plate studied has a $[0/90/\pm(\theta)]_{6s}$ laminate stacking sequence with a thickness/length ratio of 0.02 and is clamped along all edges. The effect of lamination layup on the buckling and postbuckling behavior of the structure is analyzed by varying the value of the angle θ from 0^o to 90^o in the $[0/90/\pm(\theta)]_{6s}$ laminate system, for a stress-biaxiality ratio of 2 (Fig. 25). The prebuckling stiffness is significantly reduced with increasing θ while the drop in the postbuckling stiffness is relatively smaller. The interesting result is that the buckling load (given by the linearized buckling analyses performed to construct the imperfections used in the subsequent postbuckling analyses) differs only by 2.8% from the maximum value for $\theta = 0^o$ to the minimum value for $\theta = 90^o$. For such clamped plates the optimum lamination in terms of prebuckling stiffness, buckling load and postbuckling stiffness corresponds to $\theta = 0^o$ but no drastic difference is shown while changing the lamination variable.

4.2. TRANSVERSE SHEAR DEVELOPMENT IN POSTBUCKLING

The composite plate considered is a $[0/90/\pm45]_{12s}$ clamped plate with a thickness/length ratio of 0.04. The mesh refinement performed for this composite plate to validate the solution convergence on the transverse shear

in the buckling and postbuckling analyses results in an optimized mesh of 81 elements (see Sec. 3.2.). This mesh is used in the following analyses.

4.2.1. Imperfection sensitivity

The imperfection sensitivity on transverse shear development to the magnitude of imperfection is studied. The imperfections are made of a linear combination of the three lowest eigenmodes, which gives imperfection shapes close to the first eigenmode, as presented previously (Fig. 16). Three different magnitudes (0.1%, 1% and 10% of the laminate plate thickness, respectively) are considered. The first two imperfection sizes give the same transverse section force distributions in the postbuckling range. The larger imperfection gives the higher maximum transverse shear stresses, and slightly different stress distributions before and after buckling but the differences die out as the applied load and the out-of-plane displacement increase. Convergence is obtained beyond $Nx = 1.5\ N_{xcr}$ for these analyses (see Figs. 26-27 for the stresses at the location (x,y) = (-3,-3) (in)).

Transverse shear development is then sensitive to the magnitude of imperfection at buckling whereas it is not well in the postbuckling range. Therefore this effect may not be critical, in terms of structural failure through delamination, since transverse shear stresses are large in the postbuckling range only. Subsequent analyses make use of imperfections with similar shapes as the ones presented here and scaled to 1% of the laminate plate thickness.

4.2.2. Effect of stress-biaxiality

The potential effect of loading variables on the transverse shear stress development at buckling and in the postbuckling range is studied. In order to assess this effect, two types of in-plane compressive loading (uniaxial compression along the X-direction and biaxial compression with $N_x/N_y = 2$) are considered in combination with two types of boundary conditions (simply-supported and clamped). In the four cases studied the plates buckle in a half sine-wave in both in-plane directions. This buckling mode remains in the postbuckling range, up to $N_x = 2\ N_{xcr}$, except for the clamped plate under uniaxial compression. For this case a bifurcation occurs in an antisymmetric mode with two half sine-waves in the X-direction and one half sine-wave in the Y-direction. This case is presented previously in Sec. 4.1.1.2. to characterize the imperfection sensitivity of the structure in case of a change in buckling mode.

For each boundary condition used, the transverse section-force distributions obtained under uniaxial compression and biaxial compression are similar. In terms of maximum transverse shear forces Q_x and Q_y (Figs. 28-29) developed in buckling and postbuckling, biaxial compression gives higher transverse shear stresses than uniaxial compression for the simply-supported plate. No such conclusion can be drawn for the clamped plate before it encounters a change in buckling mode under uniaxial compression. However the transverse shear increases drastically after the change in buckling mode in this case. The new buckling mode is an antisymmetric mode made of two half sine-waves in the X-direction and one half sine-wave in the Y-direction. Therefore this points

out that the larger the number of half sine-waves the buckling mode is made of, the bigger the transverse shear stresses are.

The results presented in this study show that loading variables seem to have no direct effect on the transverse shear deformation developed in the postbuckling response.

4.2.3. Effect of boundary conditions

From the four analyses presented in the previous section, the effect of the boundary conditions on the transverse shear development in buckling and postbuckling can be analyzed. Each boundary condition considered (simply-supported or clamped) gives different transverse shear stress distributions. For the simply-supported plate the distributions of the two transverse section forces (Figs. 30-31) are symmetric while this is not the case for the clamped plate (Figs. 32-33). The maximum transverse shear forces Q_x and Q_y (Figs. 28-29) developed in buckling and postbuckling are lower with simply-supported boundary conditions than with clamped boundary conditions. Moreover, the transverse shear stresses in both directions are in the same range for the former boundary conditions, whereas for the latter ones the stresses in the Y-direction are two times larger than the ones in the X-direction (corresponding to Q_y and Q_x, respectively) for both loading conditions. This relates to the non-symmetric transverse shear stress distributions in both directions obtained for the clamped plate. Therefore the transverse shear stresses developed in the postbuckling response depend strongly on the boundary conditions in terms of stress levels as well as stress distributions.

4.3. EFFECT OF THICKNESS

The effect of laminate thickness on buckling and postbuckling behavior of composite plates is studied for $[0/90/\pm45]_{ns}$ clamped plates under biaxial compression ($N_x/N_y = 2$). Four thickness/length ratios are considered: 0.02, 0.04, 0.06, 0.08. The first and last ratios correspond to the composite plates analyzed in Sec. 3.2. to assess the solution convergence. The mesh refinements performed in this previous study result in a 5x5 optimal finite-element mesh for the lowest thickness/length ratio and a 9x9 mesh for the largest one. The last mesh is used for two other thickness/length ratios (0.04, 0.06) considered in this analysis.

4.3.1. Global load-deformation response during buckling and postbuckling

Linearized buckling analyses are performed to determine the three lowest buckling modes and their corresponding eigenvalues. From these three modes, imperfections (with shapes close to the first eigenmode and magnitudes equal to 1% of the plate thickness) are constructed to model the buckling and postbuckling response for each length/thickness ratio considered. To assess the effect of transverse shear on the load-deformation responses of the laminates, a load parameter (N_xL^2/D_{22}) is defined in such form that buckling would occur at the same value for all thickness/length ratios if transverse shear was not present. Likewise, the strain parameter UL/t^2 is such that all load/displacement curves are identical prior to buckling. The load/end shortening curves obtained (Fig. 34) show that increasing the laminate plate thickness reduces the non-dimensionalized buckling load and postbuckling

stiffness, due to transverse shear.

4.3.2. Buckling loads and modes

A plot of the three lowest eigenvalues for the composite buckling with different thickness/length ratios shows that increasing the laminate thickness reduces the buckling load (i.e., first eigenvalue) and higher eigenvalues (due to increasing transverse shear) (Fig. 35). Moreover, the ratios of higher eigenvalues to the first one decrease as the thickness/length ratio increases. Therefore thick-section laminates are likely to encounter changes in buckling modes or even multiple buckling modes in the postbuckling as the eigenvalues of the composite become closer together. For the composite plates studied here, the first and second modes are the same for all four thickness/length ratios (symmetric mode and antisymmmetric mode, respectively) while the third one is antisymmetric for the two smallest ratios, and symmetric for the two largest ones.

4.3.3. Postbuckling load-deformation

The postbuckling responses of the four laminates considered (Fig. 34) show that, with increasing thickness/length ratios, the postbuckling stiffness gradually decreases as the load increases (especially for t/L = 0.08). Examining the transverse displacement development, activation of higher (i.e. second and third) modes is found to take place beyond $N_x = 1.5\ N_{xcr}$ for the highest thickness/length ratio. This relates to the conclusion of the previous section which states that thick-section laminates are more likely to

encounter changes in buckling mode or multiple modes than thin laminates.

4.3.4. Interlaminar shear development

The maximum transverse shear forces Q_x and Q_y developed during buckling and postbuckling are computed for the composites with four thickness/length ratios considered. These values are normalized with respect to the in-plane force N_x as before. The results (Figs. 36-37) show that high transverse shear stresses develop rapidly at buckling and during postbuckling in thick laminates. The interlaminar stresses increase as the thickness/length ratio and the load increase, leading to the decreases in the postbuckling composite laminate stiffness pointed out previously in Secs. 4.3.1 and 4.3.3.

The rapid increase in the transverse shear force Q_x for the composite with $t/L = 0.08$ (Fig. 36) under loads beyond $N_x = 1.5\ N_{xcr}$ may be caused by the activation of the second and third modes noted previously. The same type of response can also be noticed for the case with $t/L = 0.06$ beyond $N_x = 1.7\ N_{xcr}$ and activation of higher modes may also take place for this case. This explains the gradual decrease of postbuckling stiffness with increasing load for these two cases. Therefore the development of high transverse shear stresses for thick laminates precipitates further as activation of higher modes occurs in the postbuckling range. This kind of deformation is critical for compressive load-bearing capacity of thick laminates since eigenvalues of such structures get close together as the laminate thickness/length ratio increases.

6. CONCLUSIONS

Investigation of the buckling and postbuckling behavior of thick-section composite laminates is conducted in this study. From the analyses of global load/displacement response and transverse shear development for various parameters, the following conclusions can be drawn.

The global load/displacement response of a composite laminate plate is shown to be sensitive to imperfection in the case of a change in buckling mode only. Biaxial loading reduces the postbuckling stiffness compared to uniaxial loading, for similar buckling modes. Boundary conditions have a strong effect on the buckling load and the postbuckling stiffness and this effect depends on the applied loading. On the other hand, for the $[0/90/\pm\theta]_{ns}$ laminate system studied, no effect of lamination layup on buckling and postbuckling is found.

Buckling and, especially, postbuckling induce the development of high transverse shear stresses in composite laminates. Transverse shear stress levels are sensitive to the magnitude of imperfection at buckling but this effect dies out in the postbuckling range. No direct effect of stress-biaxiality ratio on the transverse shear development during buckling and postbuckling is also found. On the other hand, boundary conditions have a strong effect on the transverse shear stress magnitudes as well as the transverse shear stress distributions. As for the global load/displacement response, this effect depends on the applied in-plane loading of the laminate.

Increasing laminate thickness is shown to reduce the buckling load and

postbuckling stiffness of composite plates, due to the development of transverse shear. Moreover, the postbuckling stiffness of thick laminates decrease as the applied load increases. This is due to the development of high transverse shear stresses in thick laminates as the load increases during postbuckling. This effect can even precipitate by activation of higher modes. Indeed, for thick laminates, the buckling loads and higher eigenvalues get close together and potential changes in buckling mode or multiple buckling modes can be obtained in postbuckling. Therefore, development of transverse shear is critical for compression load/bearing capacity of thick laminates.

7. REFERENCES

[1] D. J. Johns, Shear Buckling of Isotropic and Orthotropic Plates - A Review, British Aeronautical Research Council, Reports and Memoranda No. 3677, October 1970

[2] J. E. Ashton and T.S. Love, "Shear stability of laminated anisotropic plates", Composite Materials: Testing and Design, ASTM-STP-460, American Society for Testing and Materials, 1969, pp. 352-361

[3] J. M. Whitney, "Curvature effects in the buckling of symmetrically-laminated rectangular plates with transverse shear deformation", Composite Structures, Vol. 8, No. 2, 1987, pp. 85-103

[4] G. Singh and Y. V. K. Sadasiva Rao, "Stability of thick angle-ply composite plates", Computers and Structures, Vol. 29, No. 2, 1988, pp. 317-322

[5] D. R. J. Owen and Z. H. Li, "A refined analysis of laminated plates by finite element displacement methods - I. Fundamentals and static analysis, and - II. Vibration and stability, Computers and Structures, Vol. 26, No. 6, 1987, pp. 907-923

[6] T. H. H. Pian, "Derivation of element stiffness matrices by assumed stress distribution, AIAA Journal, Vol. 2, 1964, pp. 1333-1336

[7] M. Stein, "Effects of transverse shearing flexibility on Postbuckling of plates in shear, AIAA Journal, Vol. 27, No. 5, 1989, pp. 652-655

[8] A. K. Noor, M. D. Mathers and M. S. Anderson, "Exploiting symmetries for efficient postbuckling analysis of composite plates, AIAA Journal, Vol. 15, No. 1, 1976, pp. 24-32

[9] J. H. Starnes Jr. and M. Rouse, "Postbuckling and failure characteristics of selected flat rectangular graphite-epoxy plates loaded in compression", Proceedings of the 22nd AIAA/ASME/ASCE/AHS Structures, Structural Dynamics and Materials Conference, AIAA CP 811, 1981, pp. 423-434

[10] N. S. Azikov and V. V. Vasilev, "Stability and above critical behavior of compressed composite panels", Mechanics of Solids, Vol. 21, No. 5, 1986, pp. 160-166

[11] ABAQUS computer code (version 4.7), Hibbit, Karlsson and Sorensen Inc., Providence, R.I., 1989

[12] M. A. Crisfield, "A fast incremental/iterative solution procedure that handles "snap-through", Computers and Structures, Vol. 13, No. 1, 1981, pp. 55-62

[13] E. Riks, "An incremental approach to the solution of snapping and buckling problems", International Journal of Solids and Structures, Vol. 15, 1979, pp. 529-551

[14] B. M. Irons, "The semiLoof shell element", Finite Elements for Thin Shells and Curved Members, Proceedings of Conference on Finite Elements Applied to Thin Shells and Curved Members, Cardiff, U.K., 1974, D. G. Aswell and R. H. Gallagher, Ed., John Wiley and Sons, London, U.K., 1976

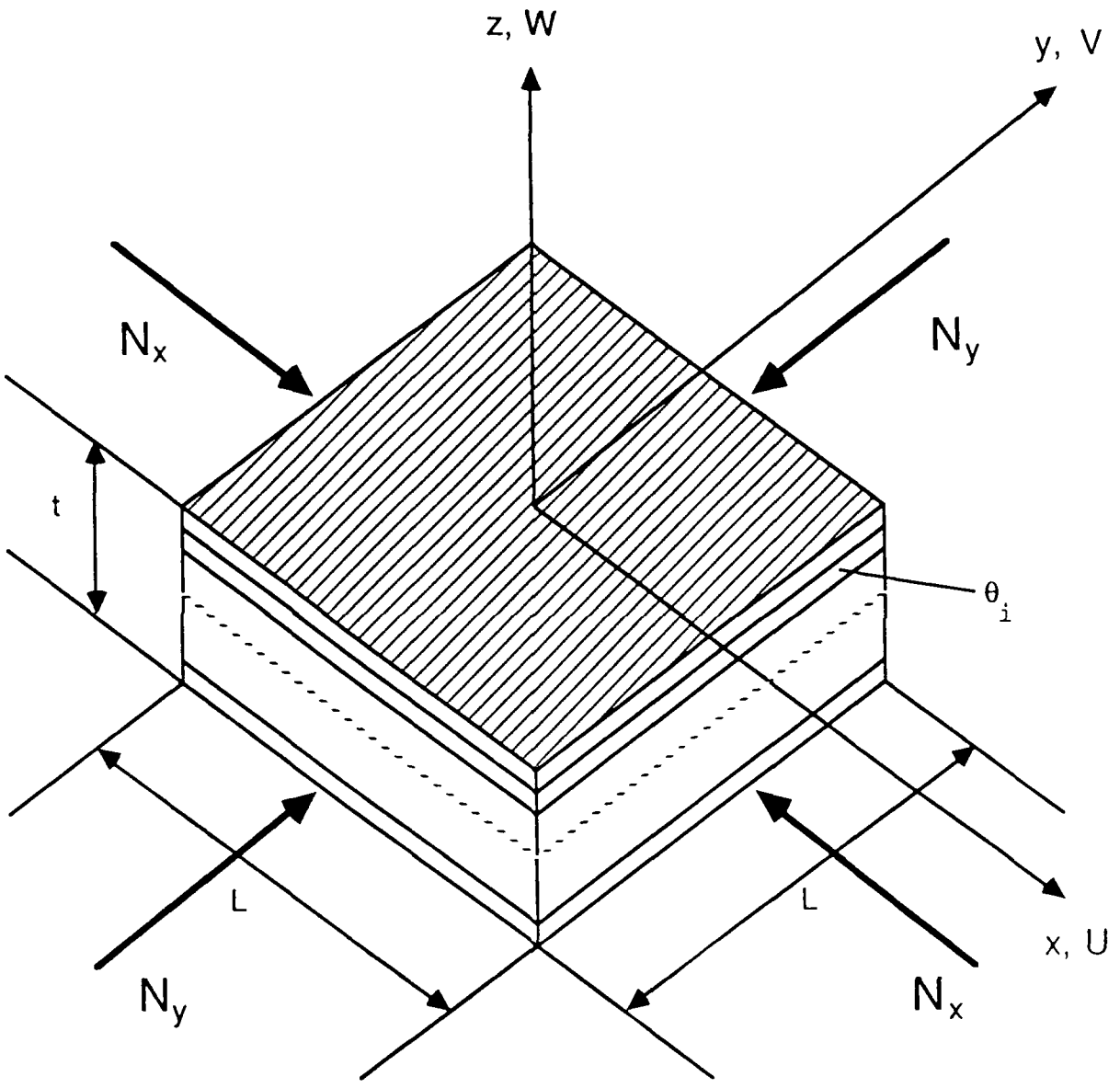

Fig. 1. Coordinates and geometry of a composite laminate plate under compressive loading

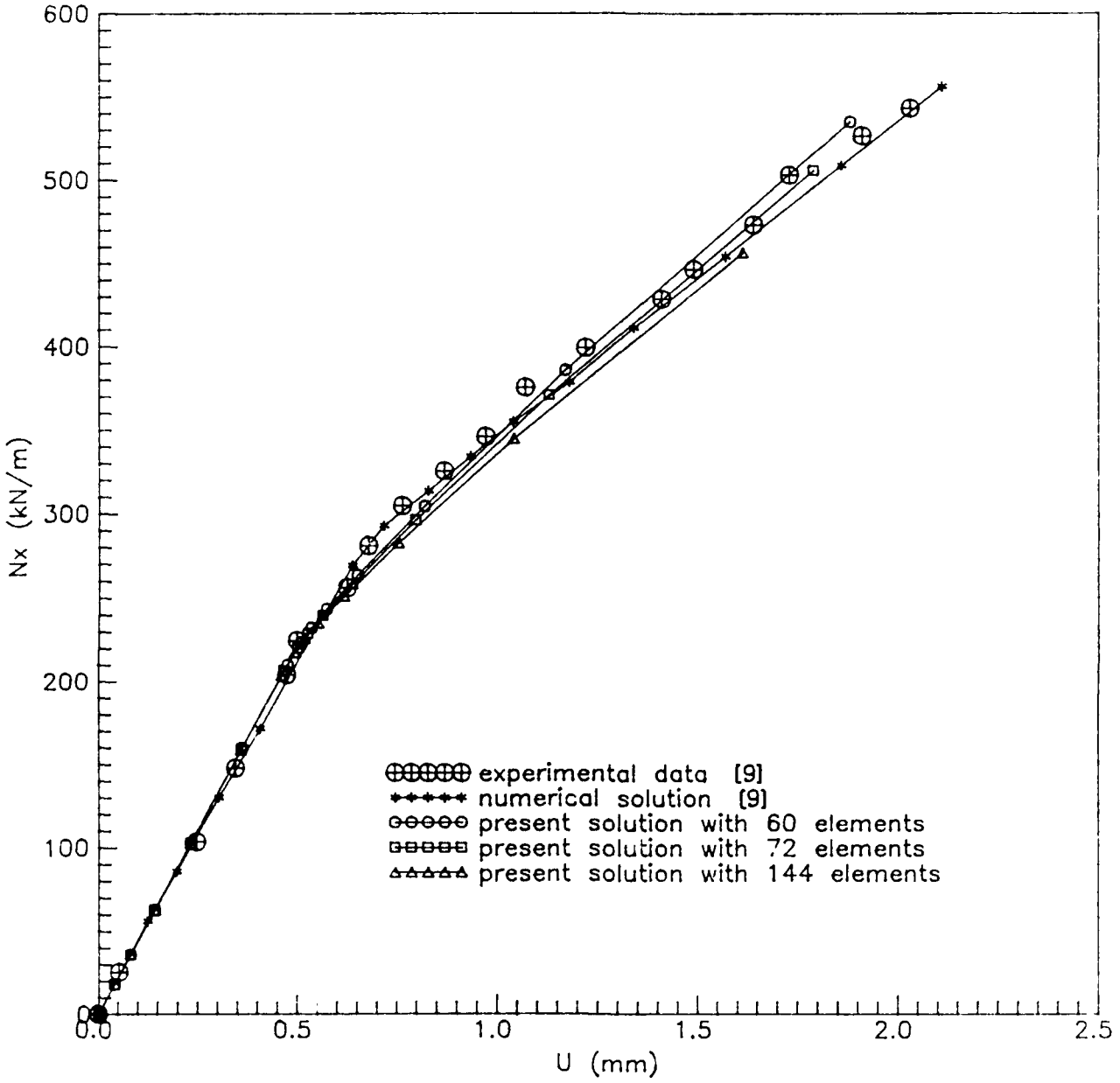

Fig. 2. Comparison among experimental data [9], current solutions (using 3-nodes triangular elements) and previous numerical results [9] for buckling and postbuckling response of a $[\pm 45/0_2/\pm 45/0_2/\pm 45/0/90]_s$ composite under uniaxial compression

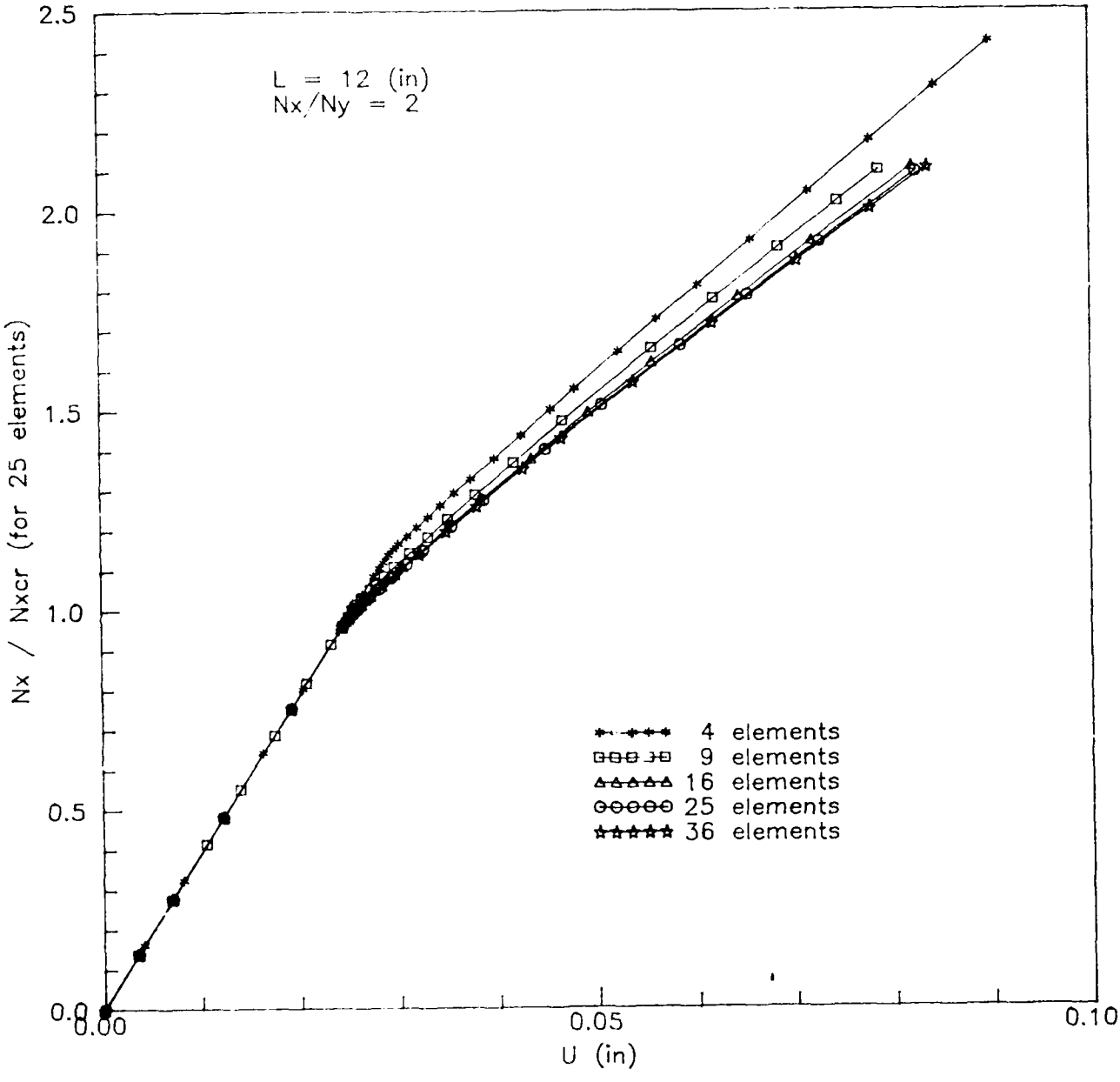

Fig. 3. Effect of mesh refinement on buckling and postbuckling solution convergence for a clamped $[0/90/\pm45]_{6s}$ plate under biaxial compression ($N_x/N_y = 2$, $t/L = 0.02$)

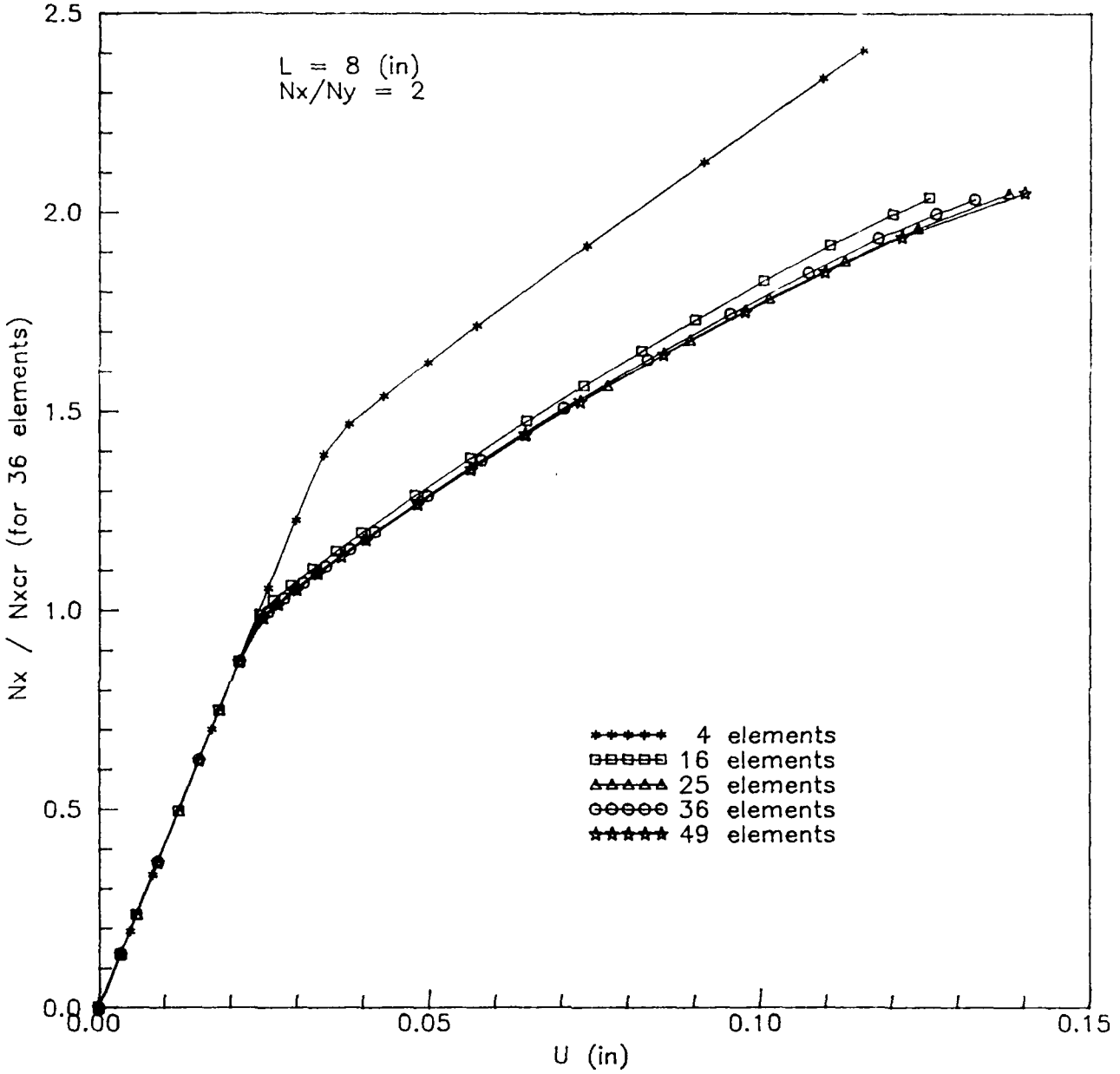

Fig. 4. Effect of mesh refinement on buckling and postbuckling solution convergence for a clamped unidirectional plate under biaxial compression ($N_x/N_y = 2$, $t/L = 0.05$)

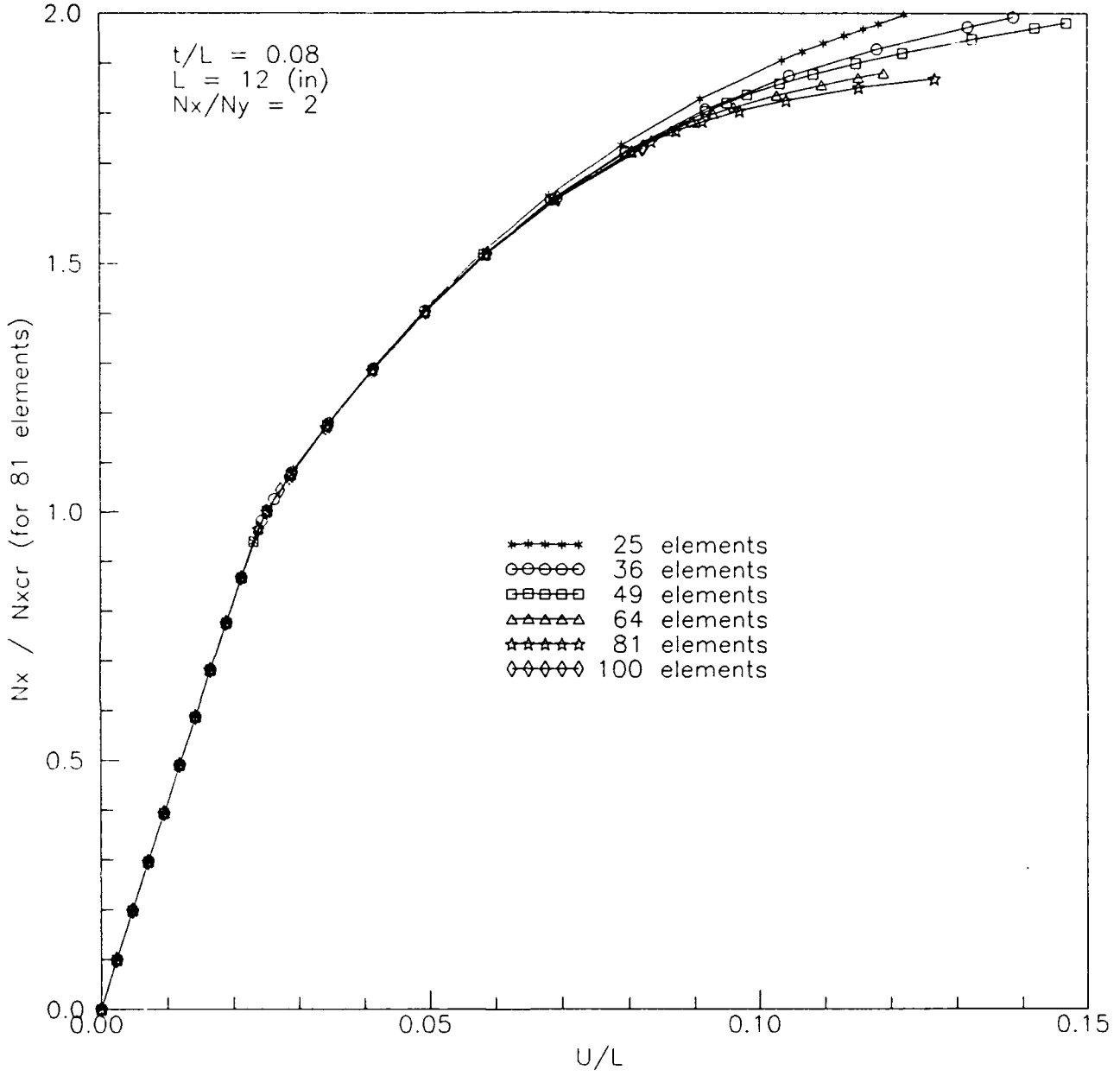

Fig. 5. Effect of mesh refinement on buckling and postbuckling solution convergence for a clamped $[0/90/\pm45]_{24s}$ plate under biaxial compression ($N_x/N_y = 2$, $t/L = 0.08$)

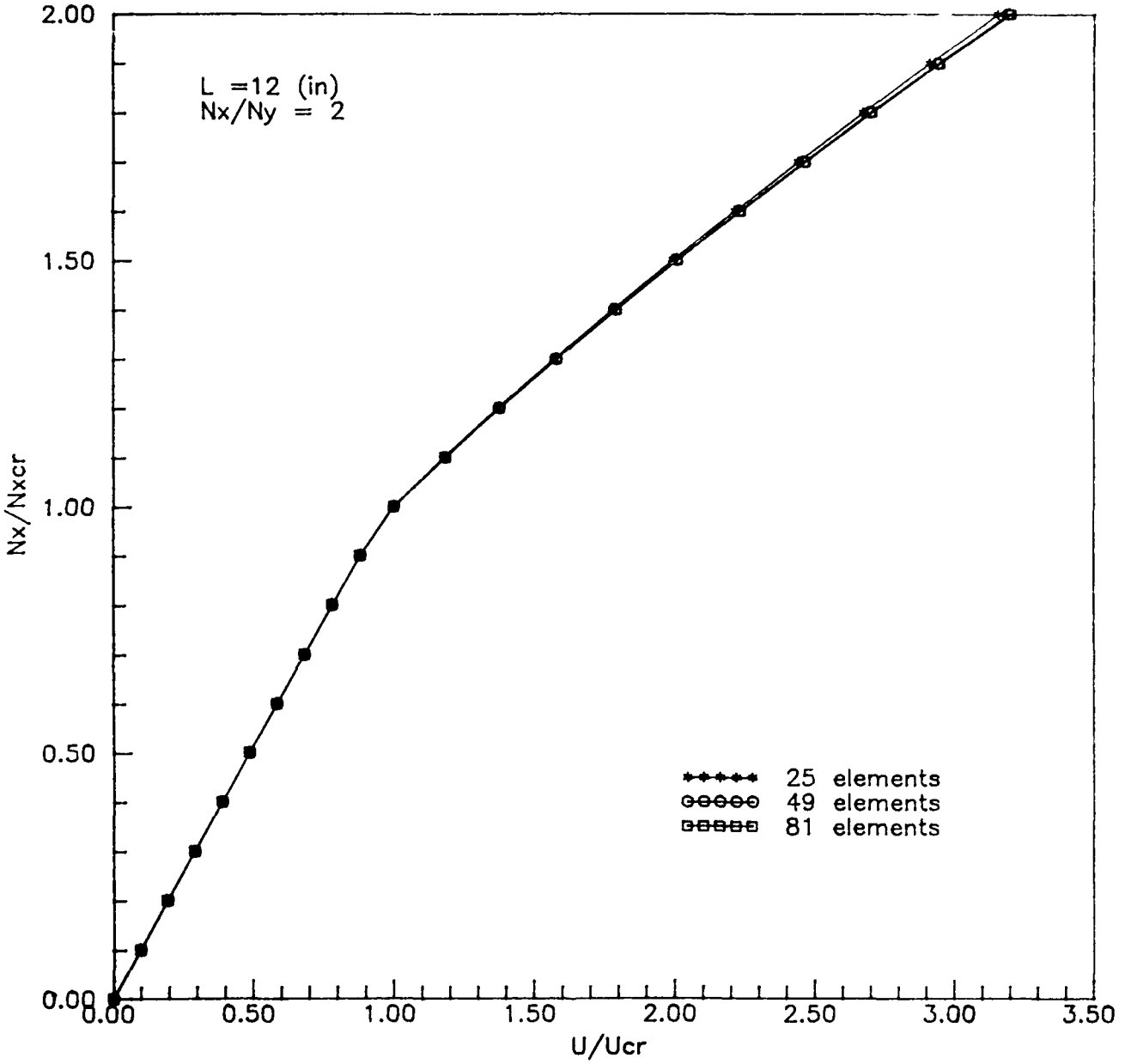

Fig. 6. Effect of mesh refinement on buckling and postbuckling solution convergence for a clamped $[0/90/\pm45]_{12s}$ plate under biaxial compression ($N_x/N_y = 2$, $t/L = 0.04$)

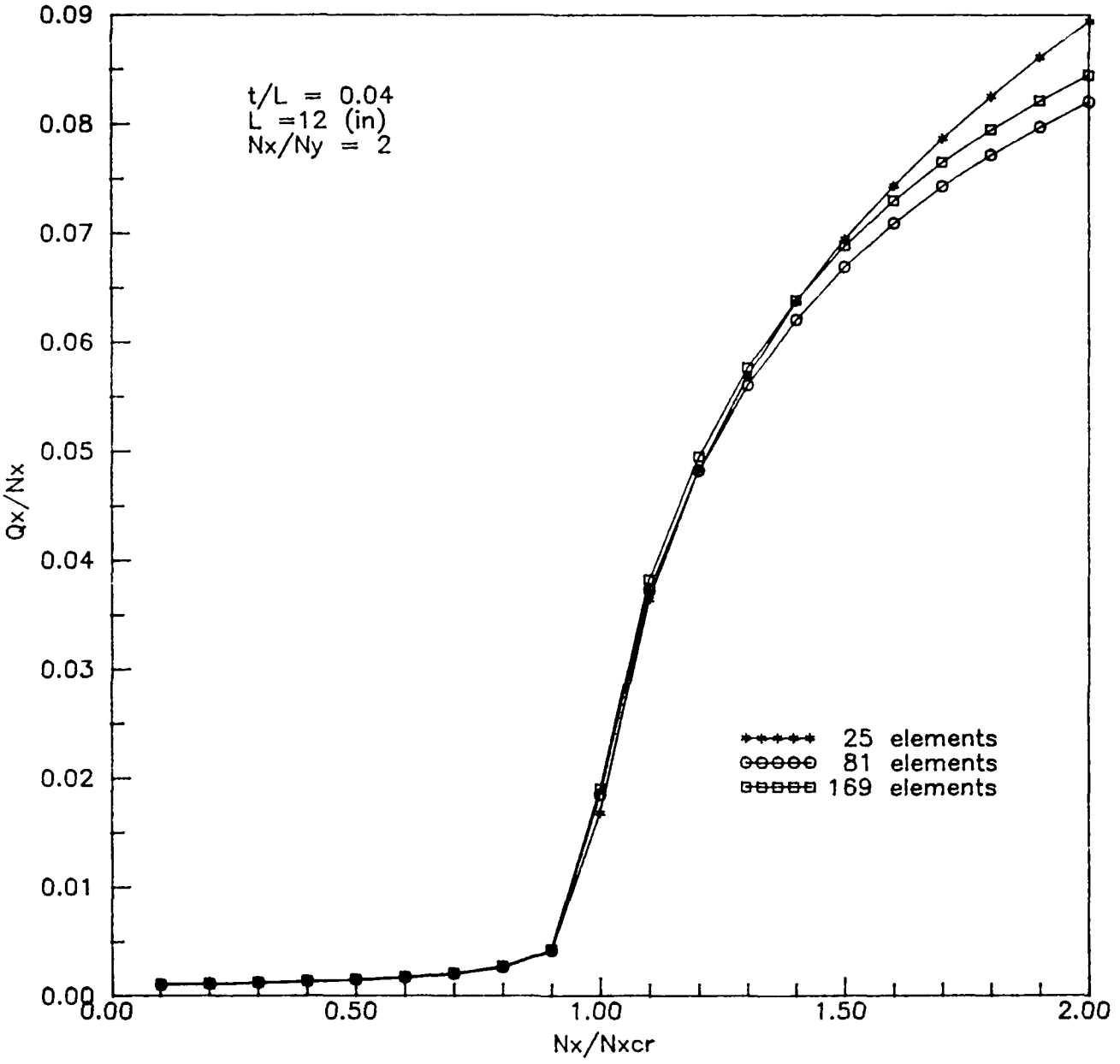

Fig. 7. Solution convergence for transverse shear Q_x at (-3,-3) (in) in a clamped $[0/90/\pm45]_{12s}$ plate under biaxial compression ($N_x/N_y = 2$, $t/L = 0.04$)

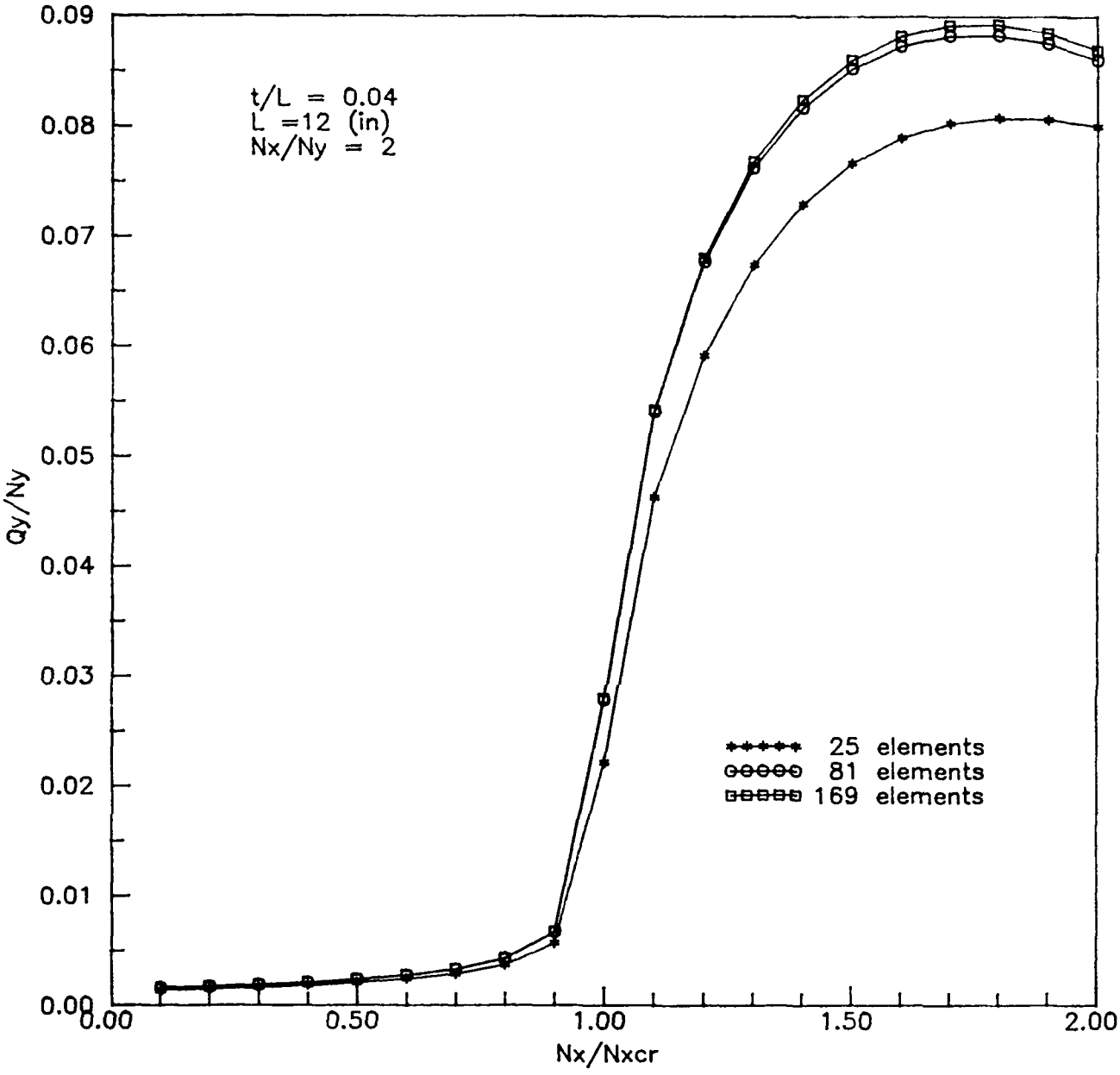

Fig. 8. Solution convergence for transverse shear Q_y at (-3,-3) (in) in a clamped $[0/90/\pm45]_{12s}$ plate under biaxial compression ($N_x/N_y = 2$, $t/L = 0.04$)

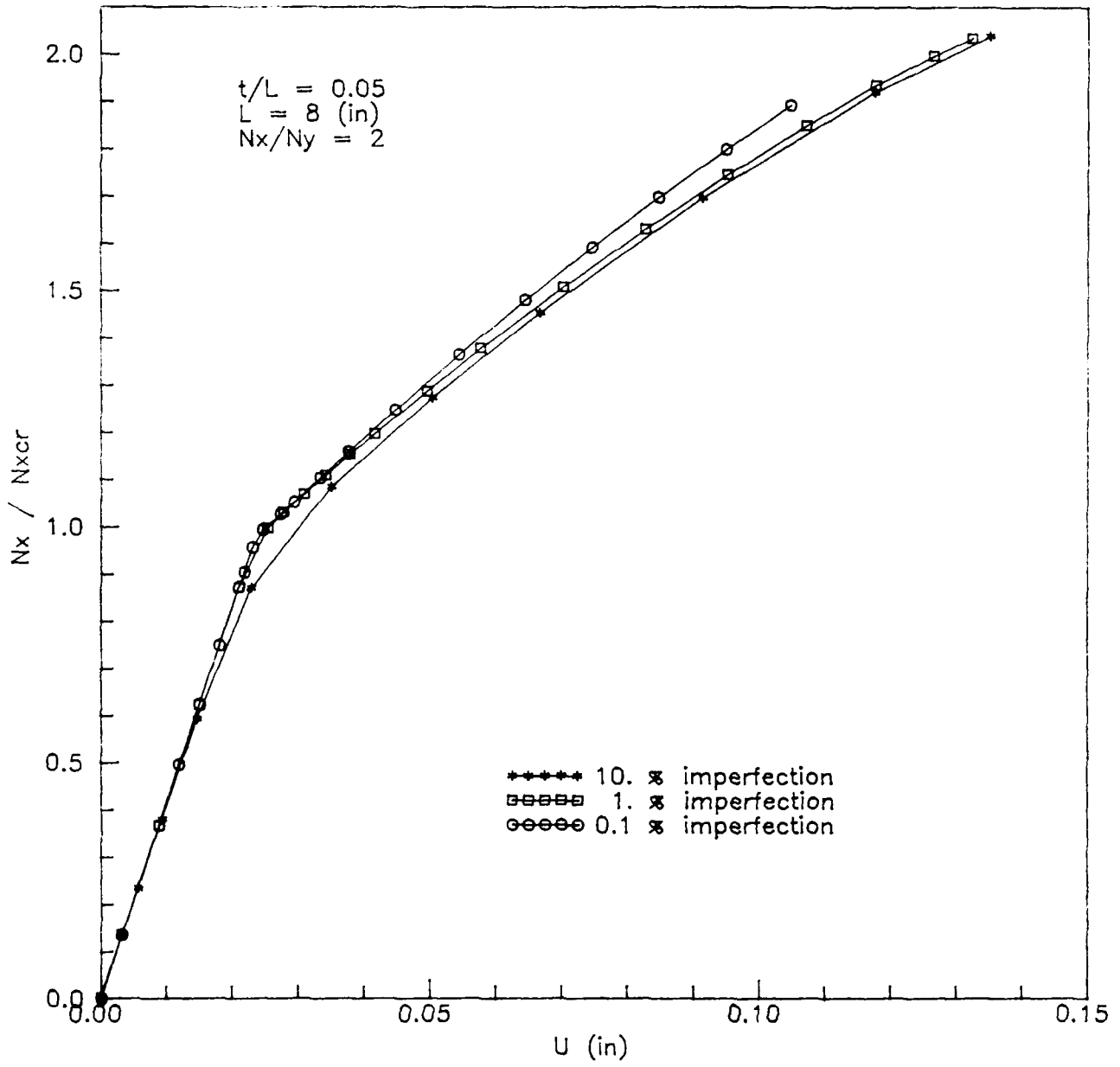

Fig. 9. Effect of imperfection sensitivity on buckling and postbuckling response of a clamped unidirectional composite plate under biaxial compression (N_x/N_y = 2, t/L = 0.05)

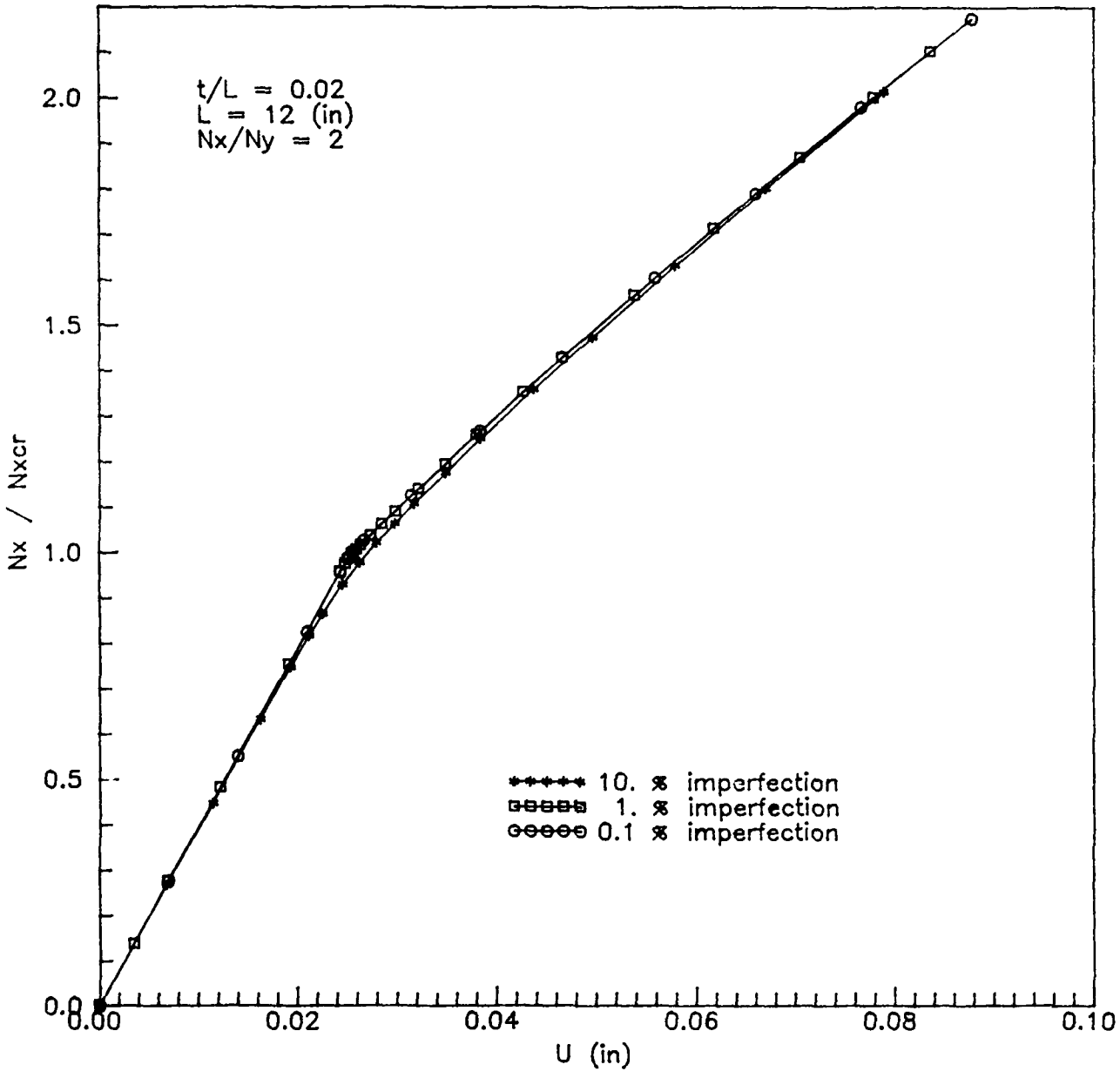

Fig. 10. Effect of imperfection sensitivity on buckling and postbuckling response of a clamped $[0/90/\pm45]_{6s}$ plate under biaxial compression ($N_x/N_y = 2$, $t/L = 0.02$)

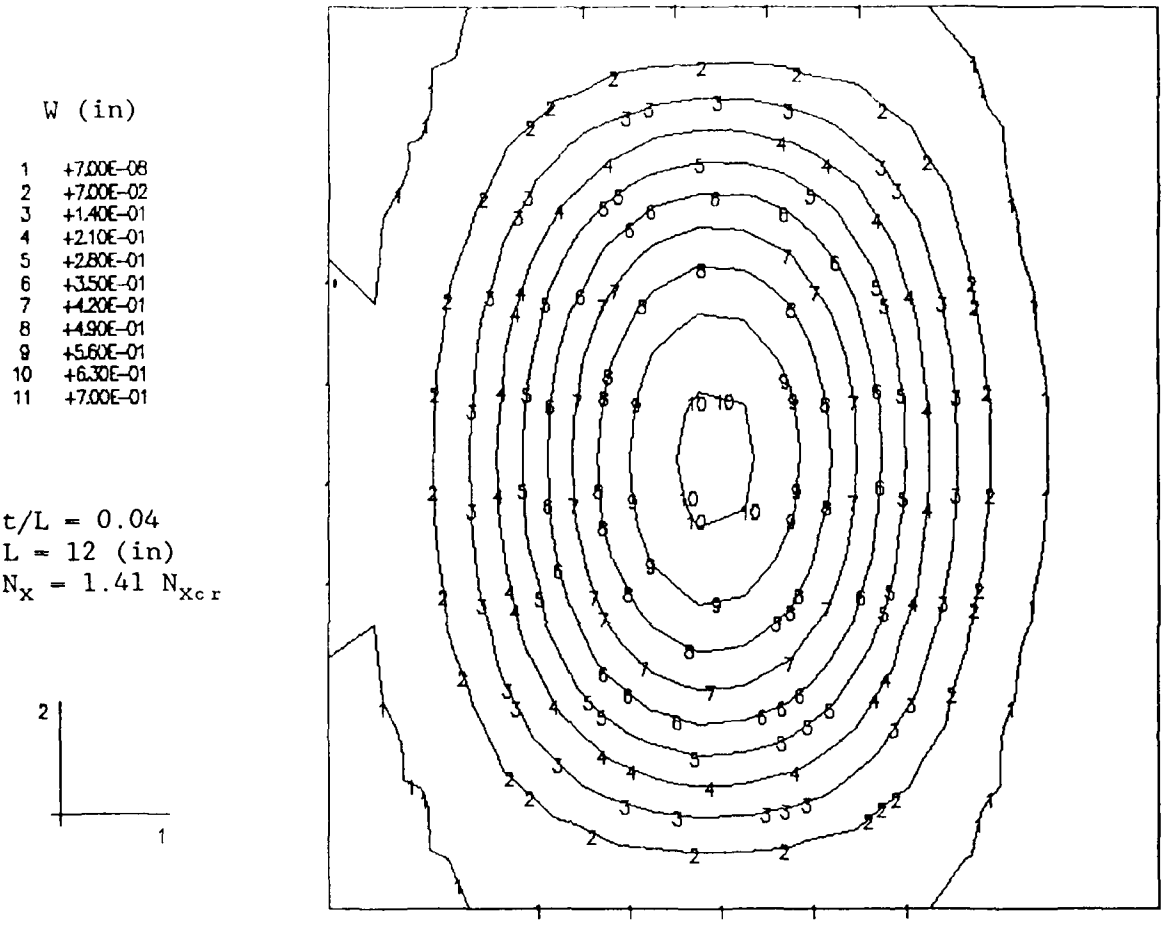

Fig. 11. Transverse displacements distribution before a change in buckling mode for a clamped $[0/90/\pm45]_{12s}$ plate under uniaxial compression ($N_x = 1.41\ N_{xcr}$, 1% imperfection, t/L = 0.04)

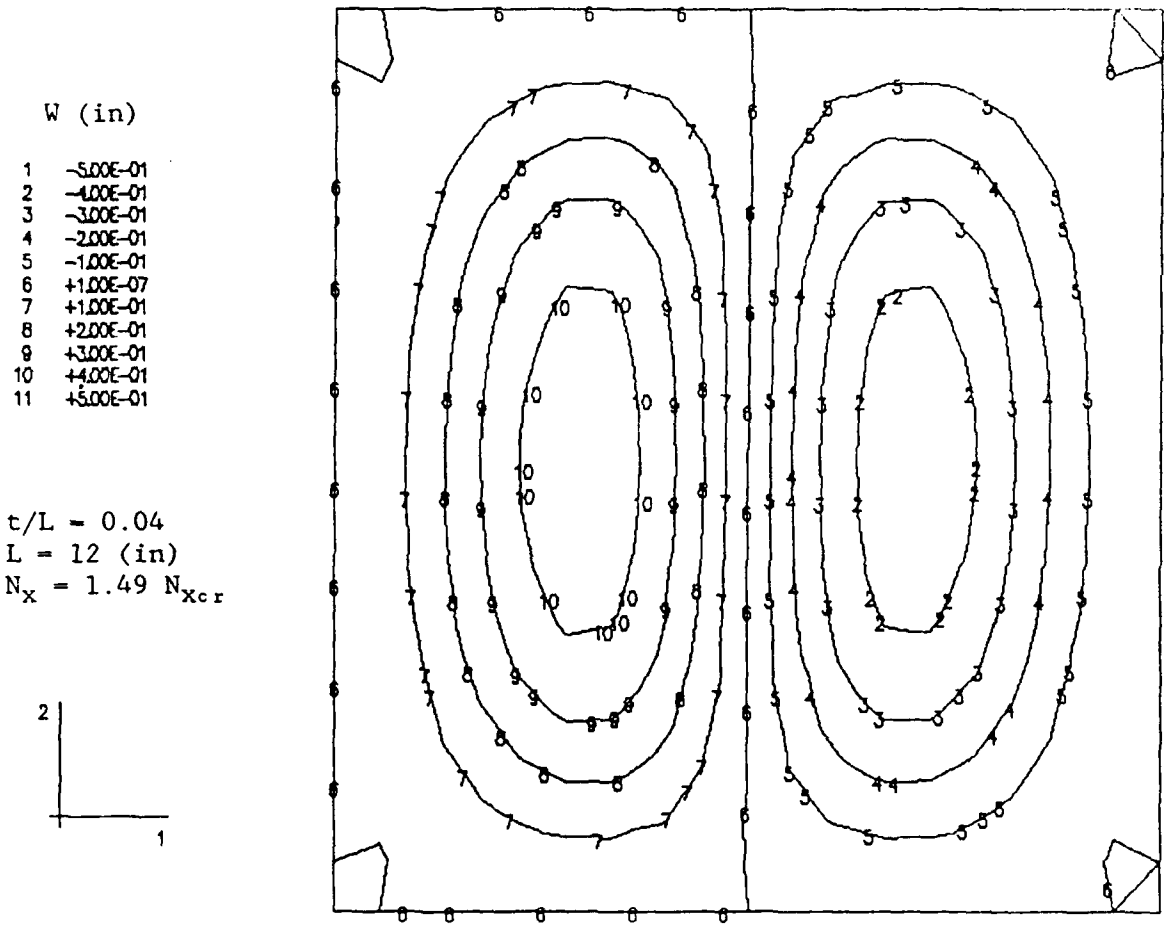

Fig. 12. Transverse displacements distribution after a change in buckling mode for a clamped $[0/90/\pm45]_{12s}$ plate under uniaxial compression ($N_X = 1.49\ N_{Xcr}$, 1% imperfection, t/L = 0.04)

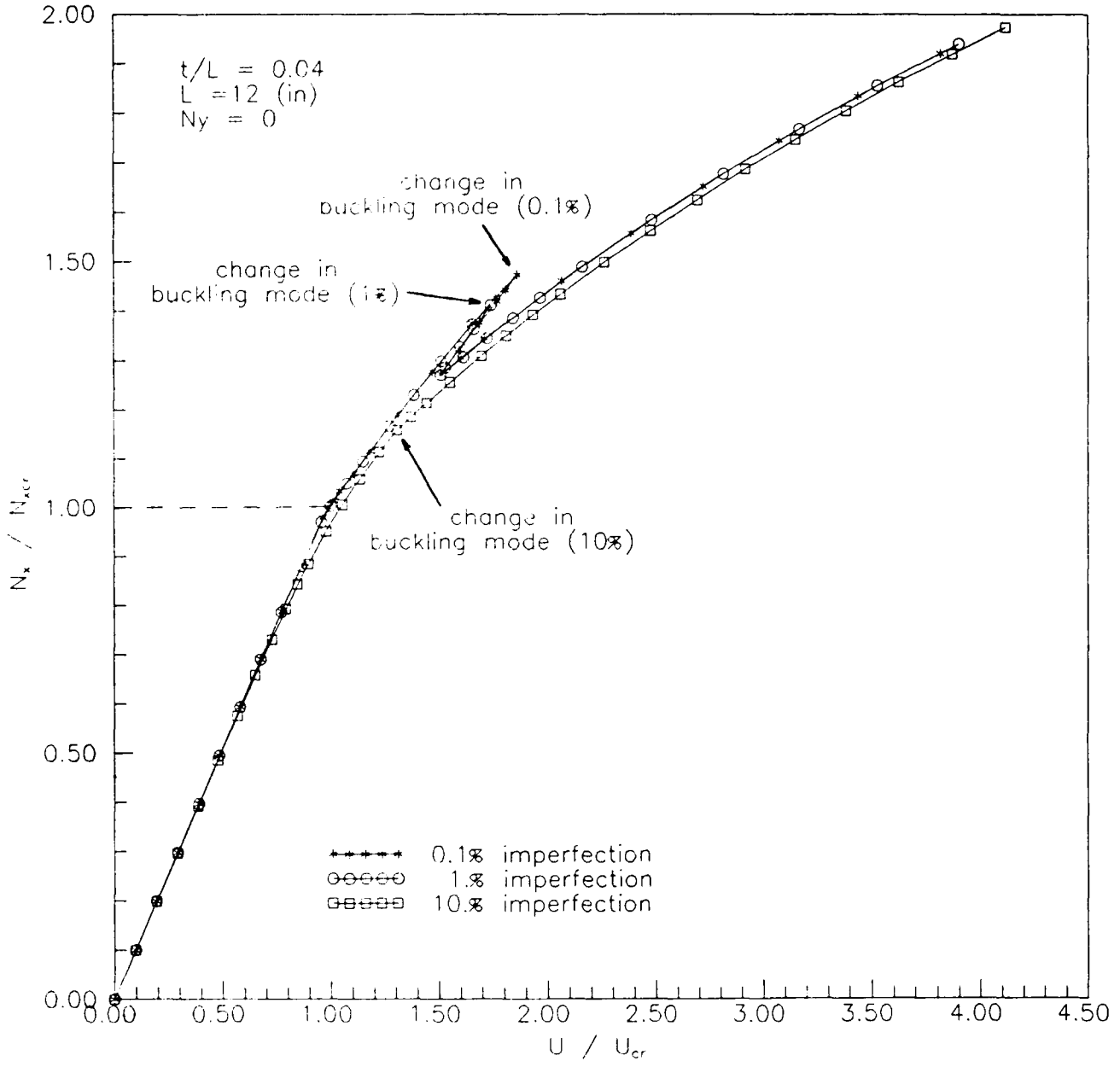

Fig. 13. Effect of imperfection sensitivity on buckling and postbuckling response (with a change in buckling mode) of a clamped $[0/90/\pm45]_{12s}$ plate under uniaxial compression ($N_y = 0$, $t/L = 0.04$)

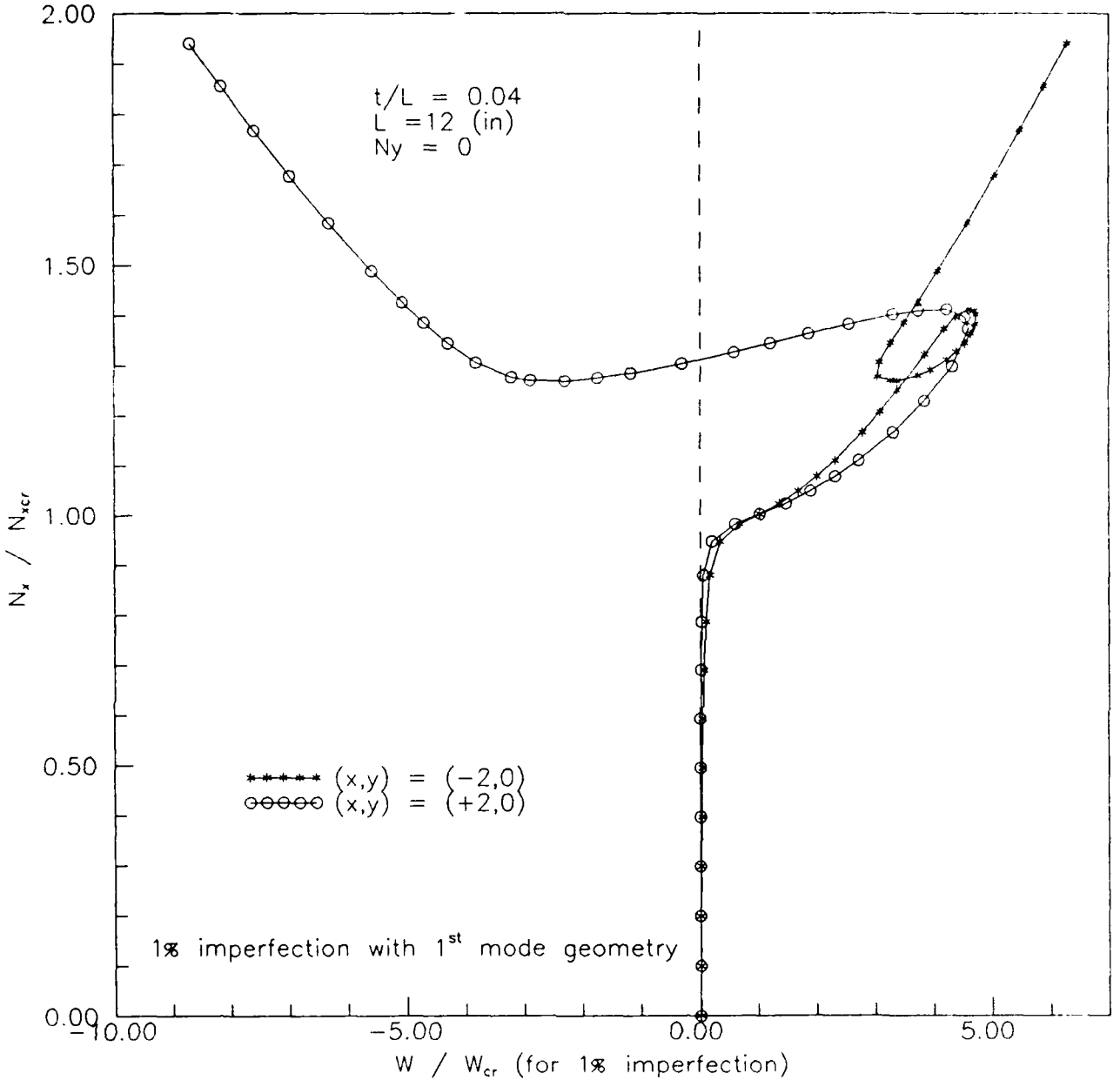

Fig. 14. Transverse displacements W at (±2,0) for a clamped $[0/90/\pm45]_{12s}$ plate under uniaxial compression (1% imperfection, $N_y = 0$, $t/L = 0.04$)

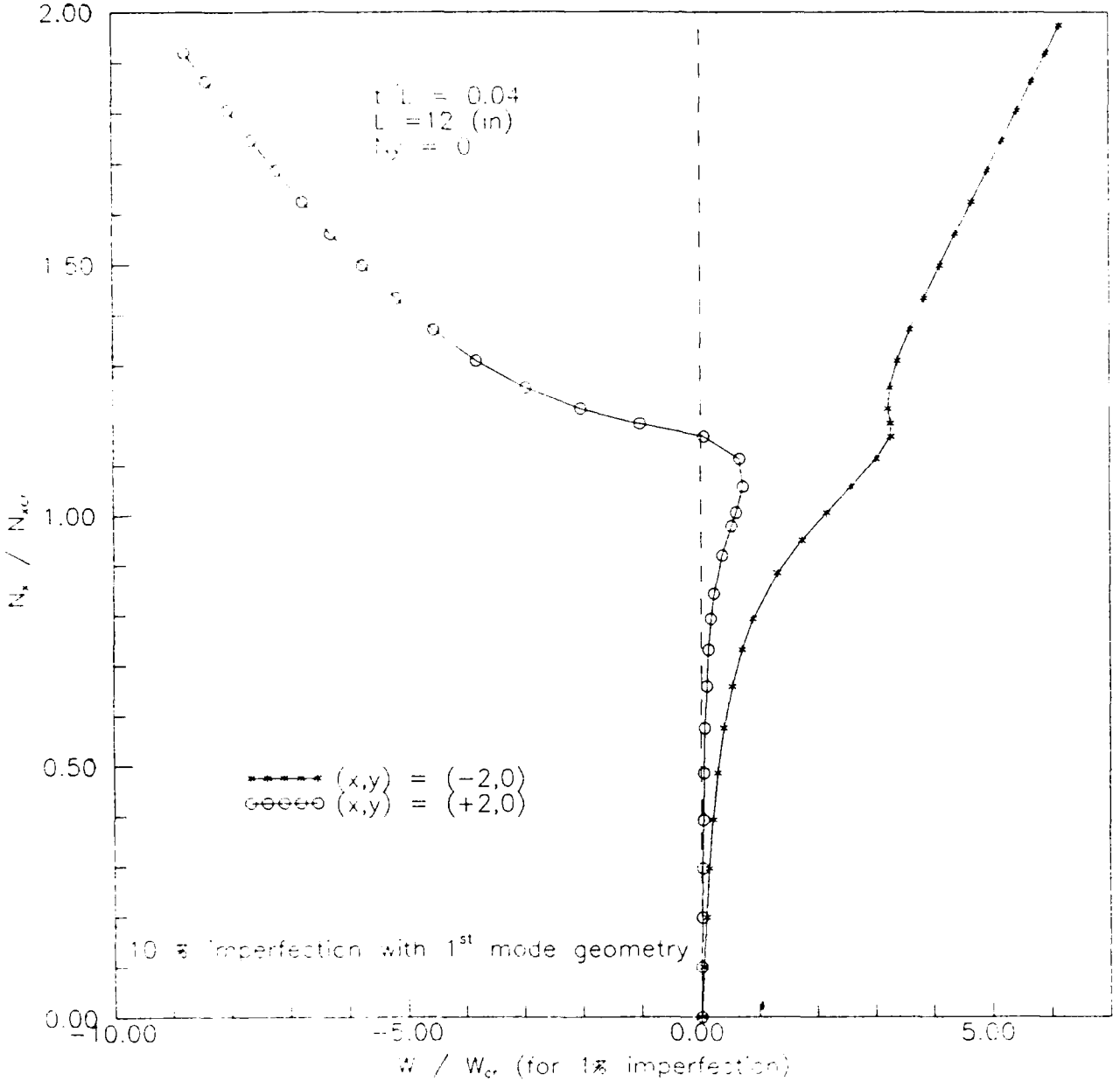

Fig. 15. Transverse displacements W at (±2,0) for a clamped $[0/90/\pm45]_{12s}$ plate under uniaxial compression (10% imperfection, $N_y = 0$, $t/L = 0.04$)

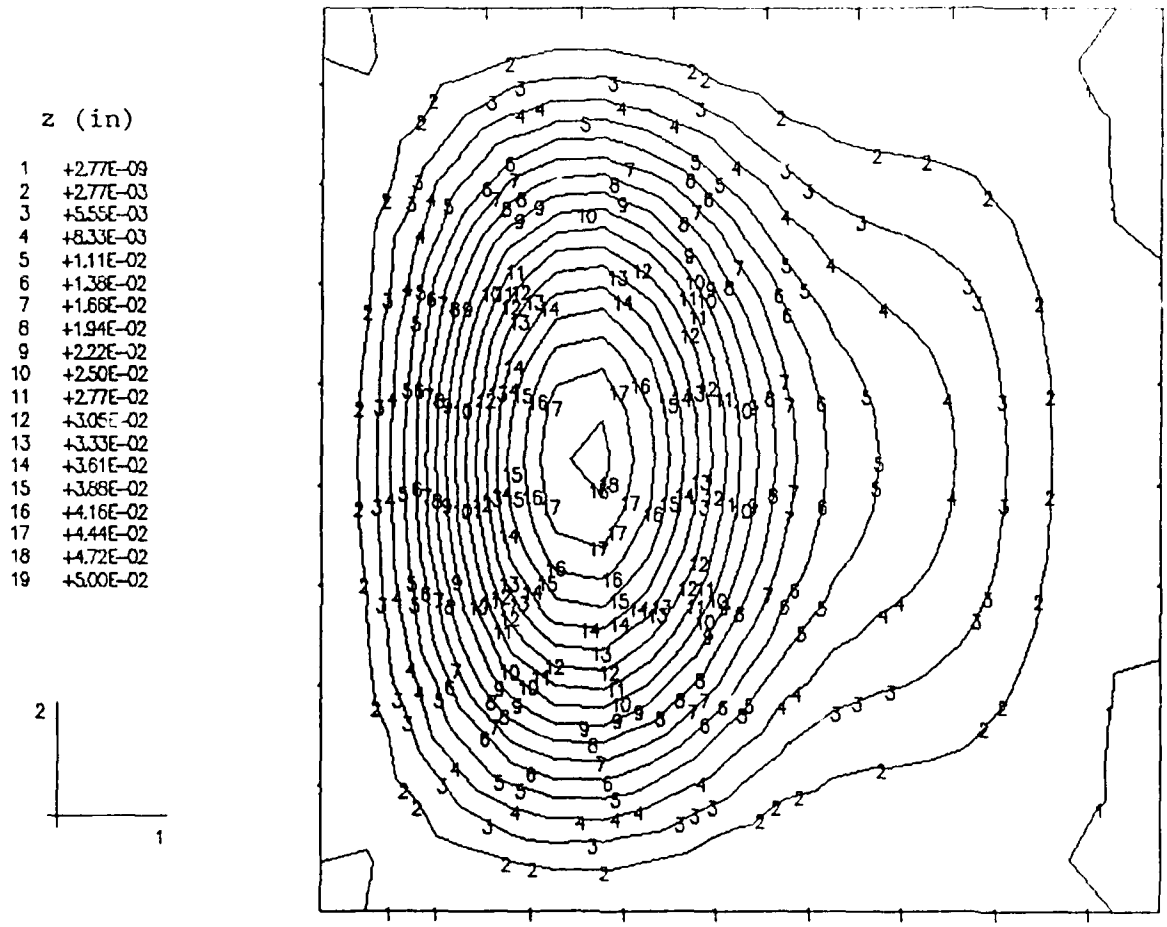

Fig. 16. Constructed imperfection geometry close to the first eigenmode for a 10% imperfection

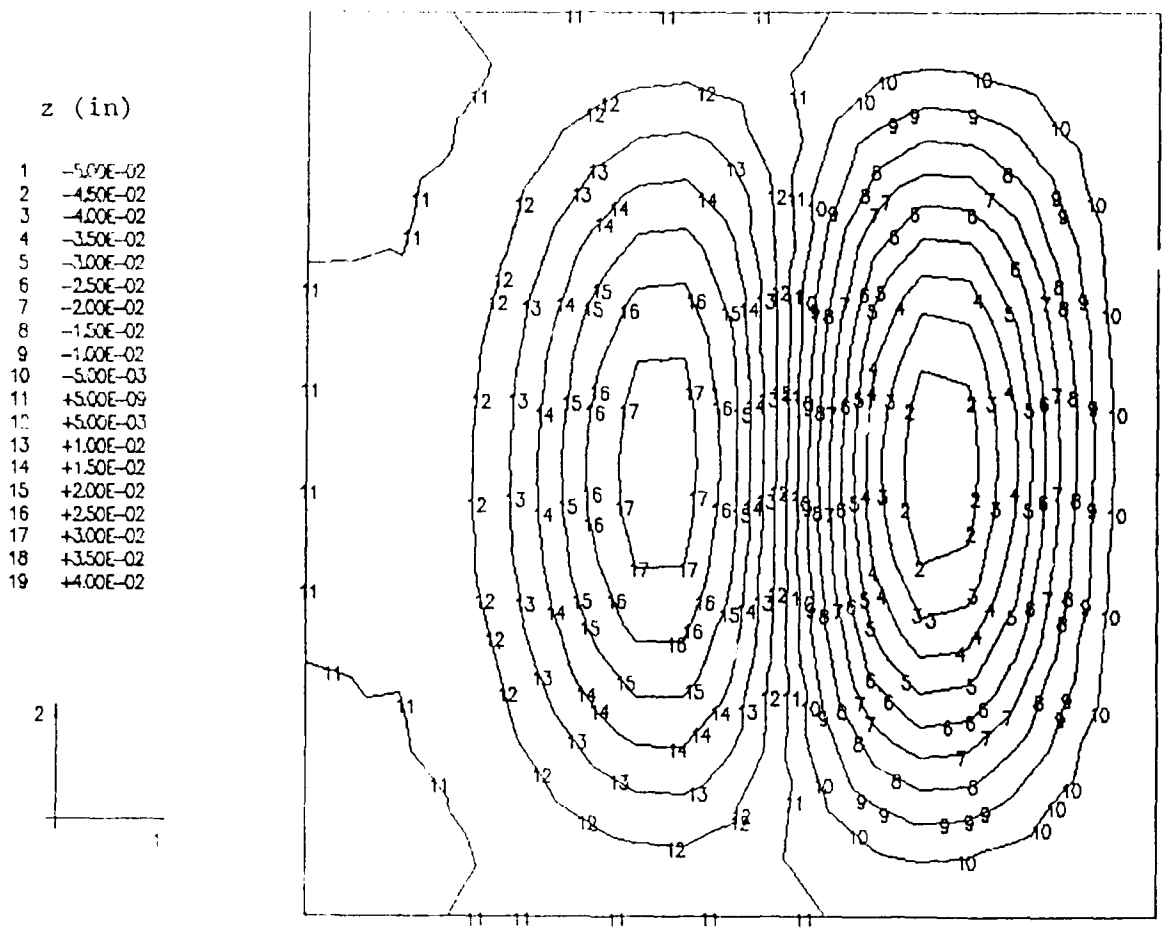

Fig. 17. Constructed imperfection geometry close to the second eigenmode for a 10% imperfection

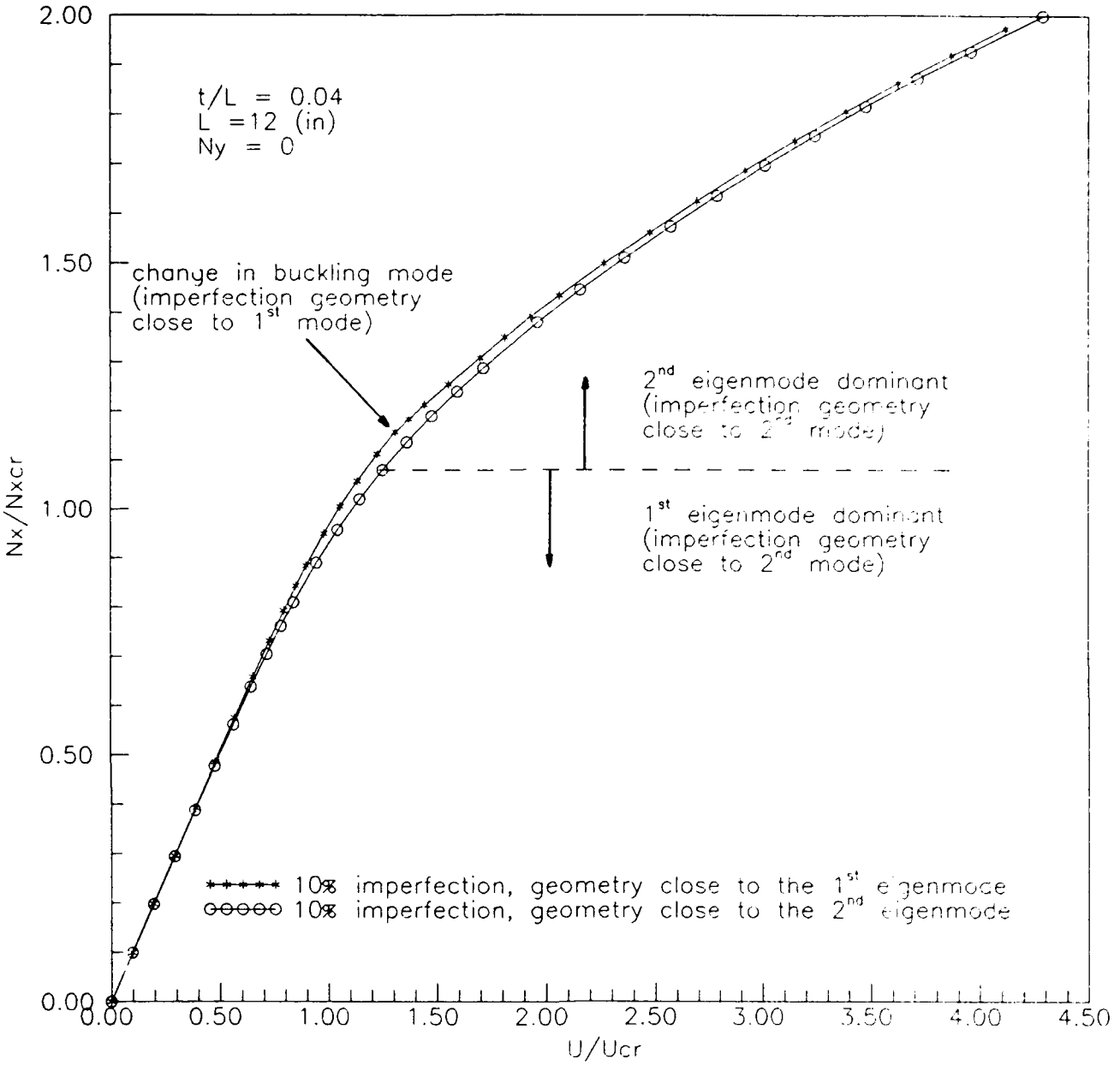

Fig. 18. Effect of imperfection geometry on buckling and postbuckling response (with a change in buckling mode) of a clamped $[0/90/\pm45]_{12s}$ plate under uniaxial compression (10% imperfection, $N_y = 0$, $t/L = 0.04$)

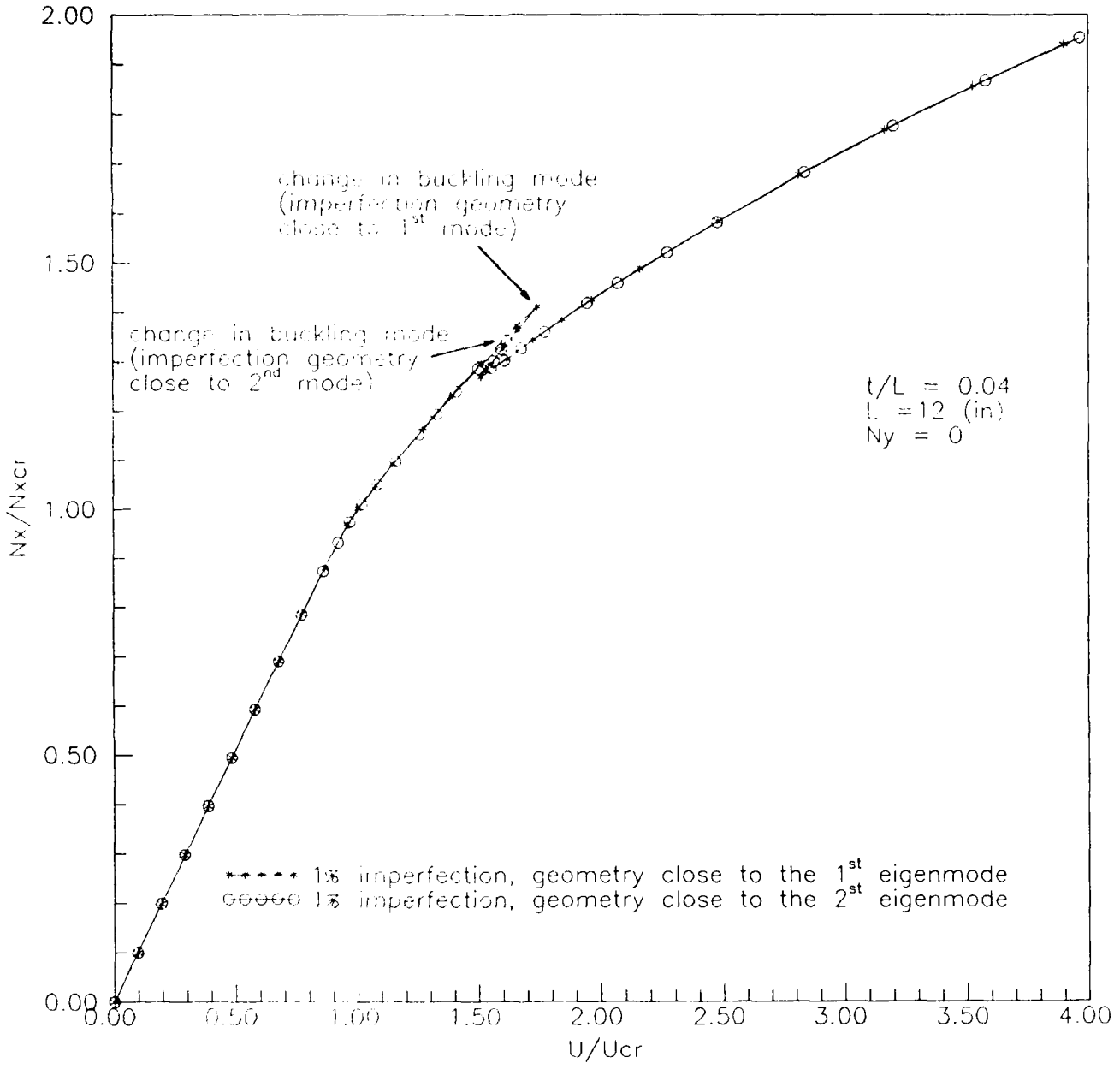

Fig. 19. Effect of imperfection geometry on buckling and postbuckling response (with a change in buckling mode) of a clamped $[0/90/\pm45]_{12s}$ plate under uniaxial compression (1% imperfection, $N_y = 0$, $t/L = 0.04$)

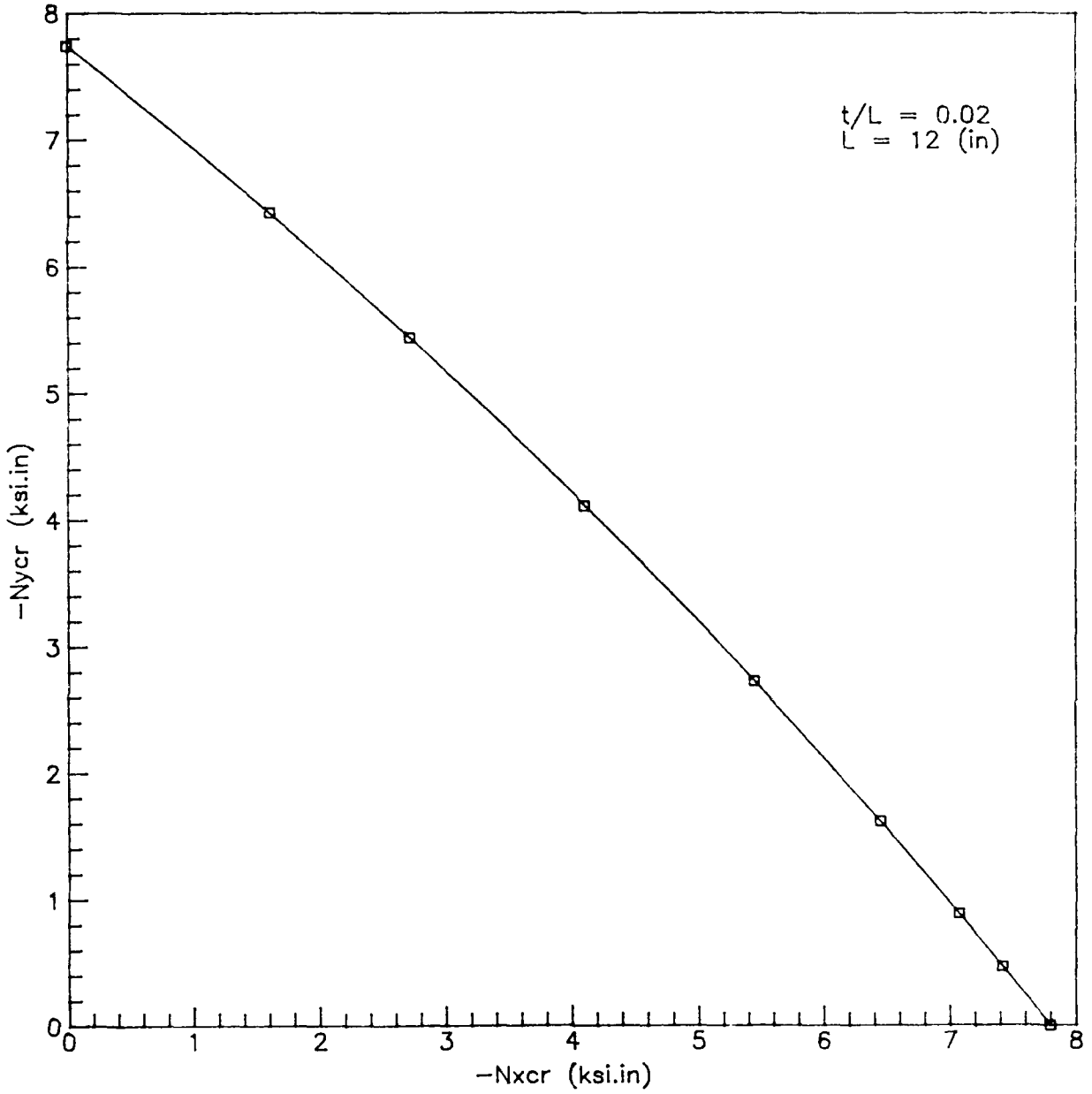

Fig. 20. Critical load-stability envelope for a clamped $[0/90/\pm45]_{6s}$ plate under biaxial states of stress (t/L = 0.02)

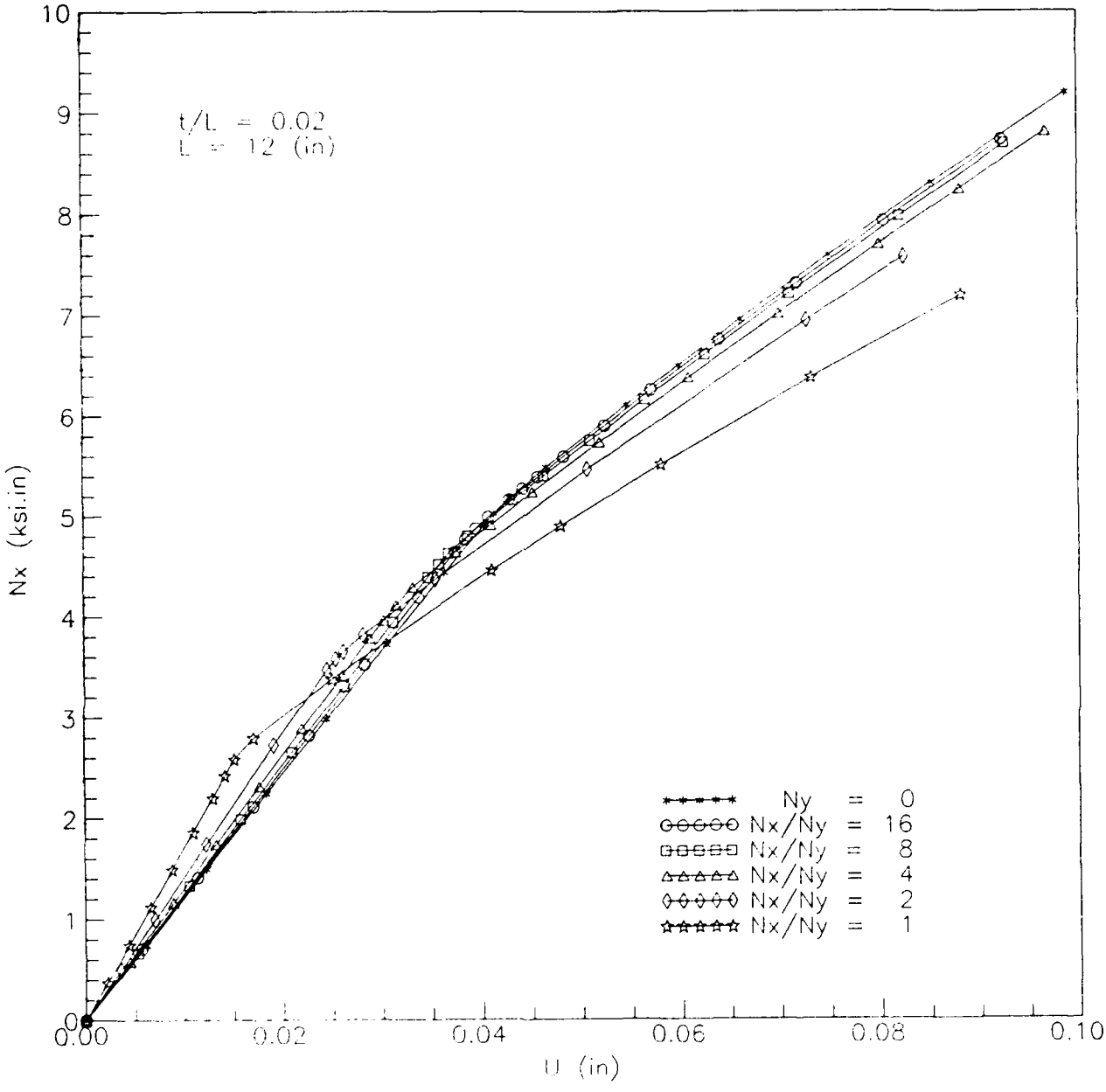

Fig. 21. Effect of stress-biaxiality ratio on buckling and postbuckling response (load N_x versus end-shortening U) along the X-axis for a clamped $[0/90/\pm45]_{6s}$ plate (t/L = 0.02)

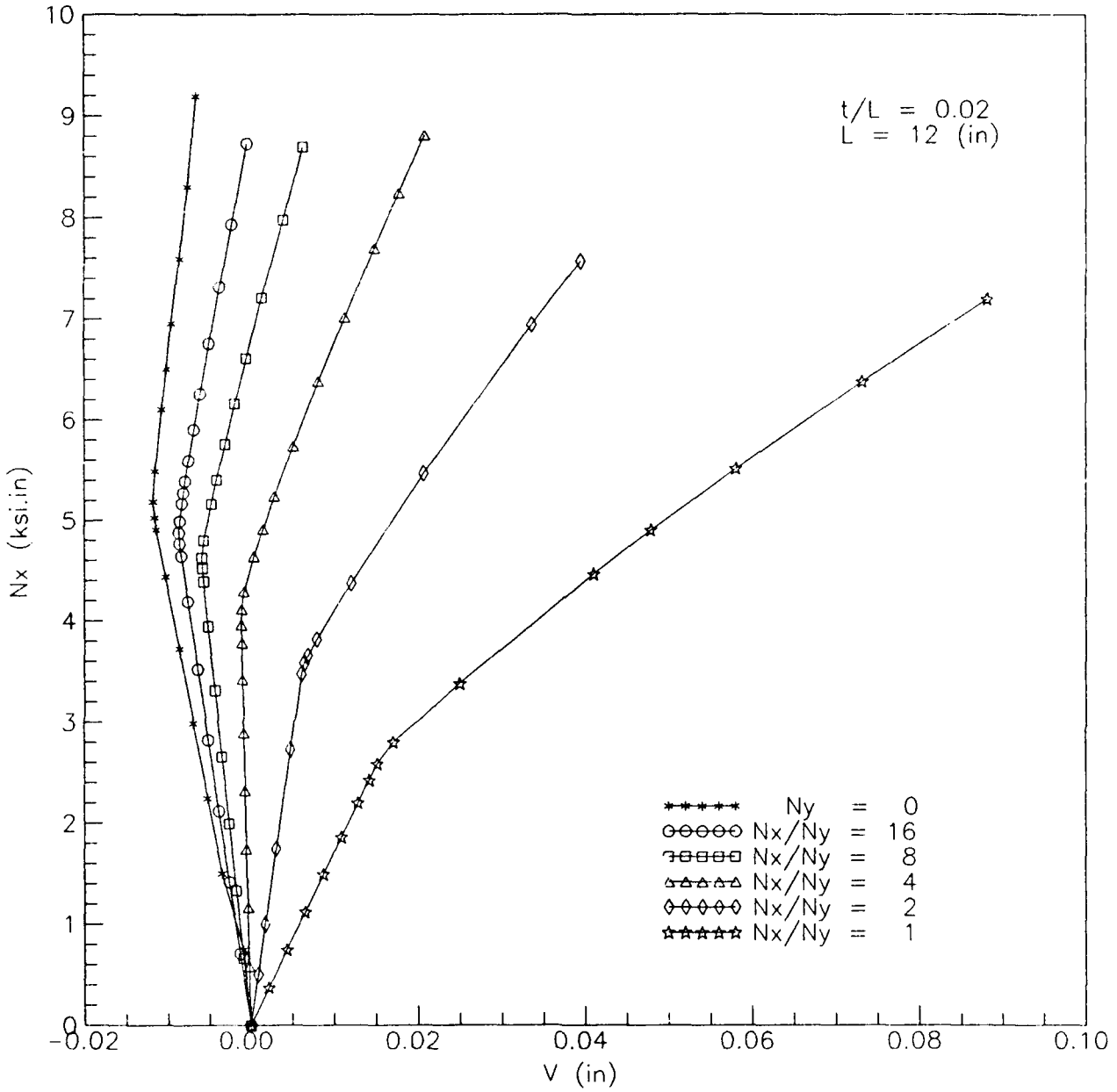

Fig. 22. Effect of stress-biaxiality ratio on buckling and postbuckling response (load N_x versus end-shortening V) along the Y-axis for a clamped $[0/90/\pm45]_{6s}$ plate (t/L = 0.02)

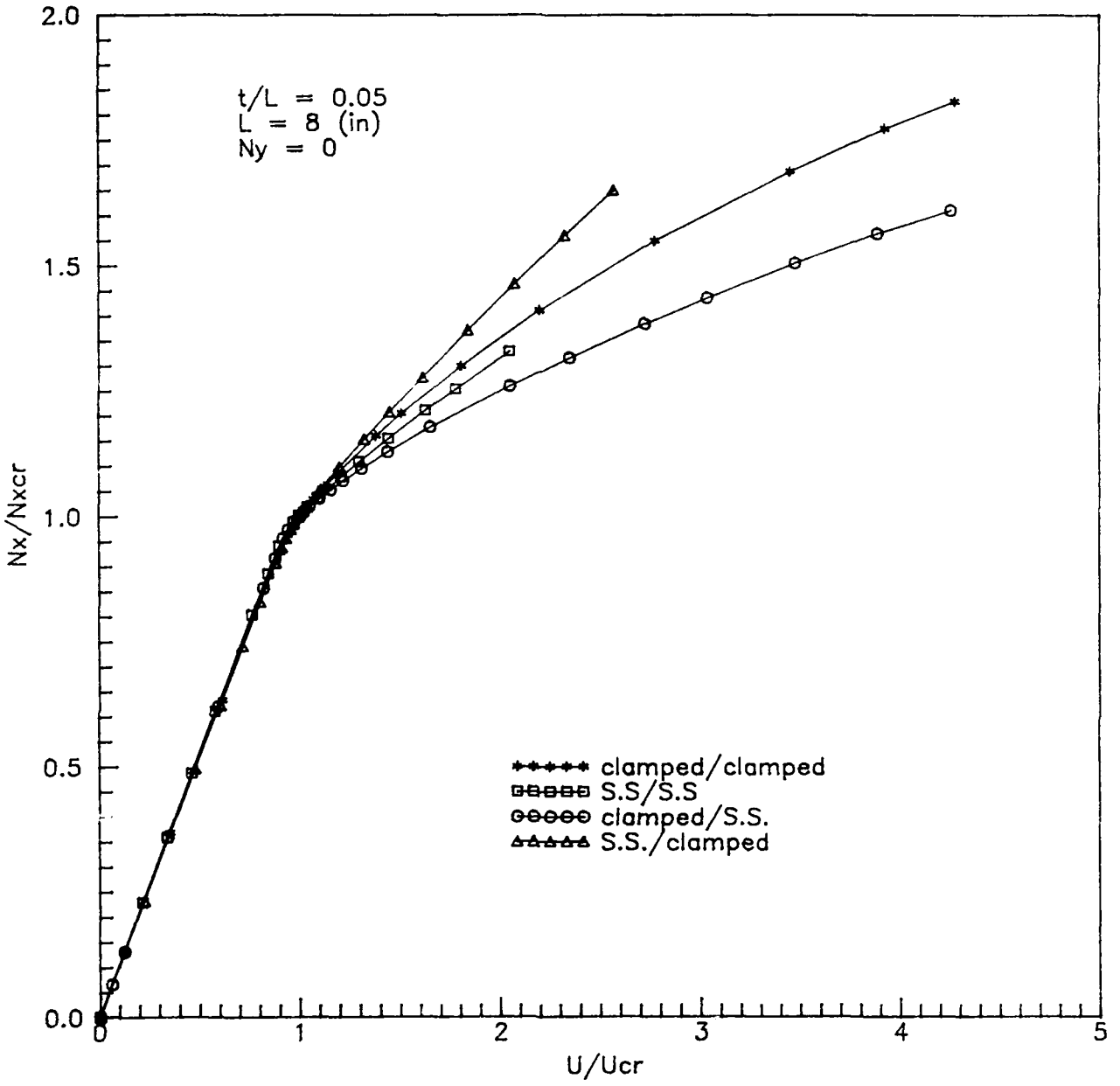

Fig. 23. Effect of boundary conditions on buckling and postbuckling response of a unidirectional laminate plate under uniaxial compression (N_y = 0, t/L = 0.05)

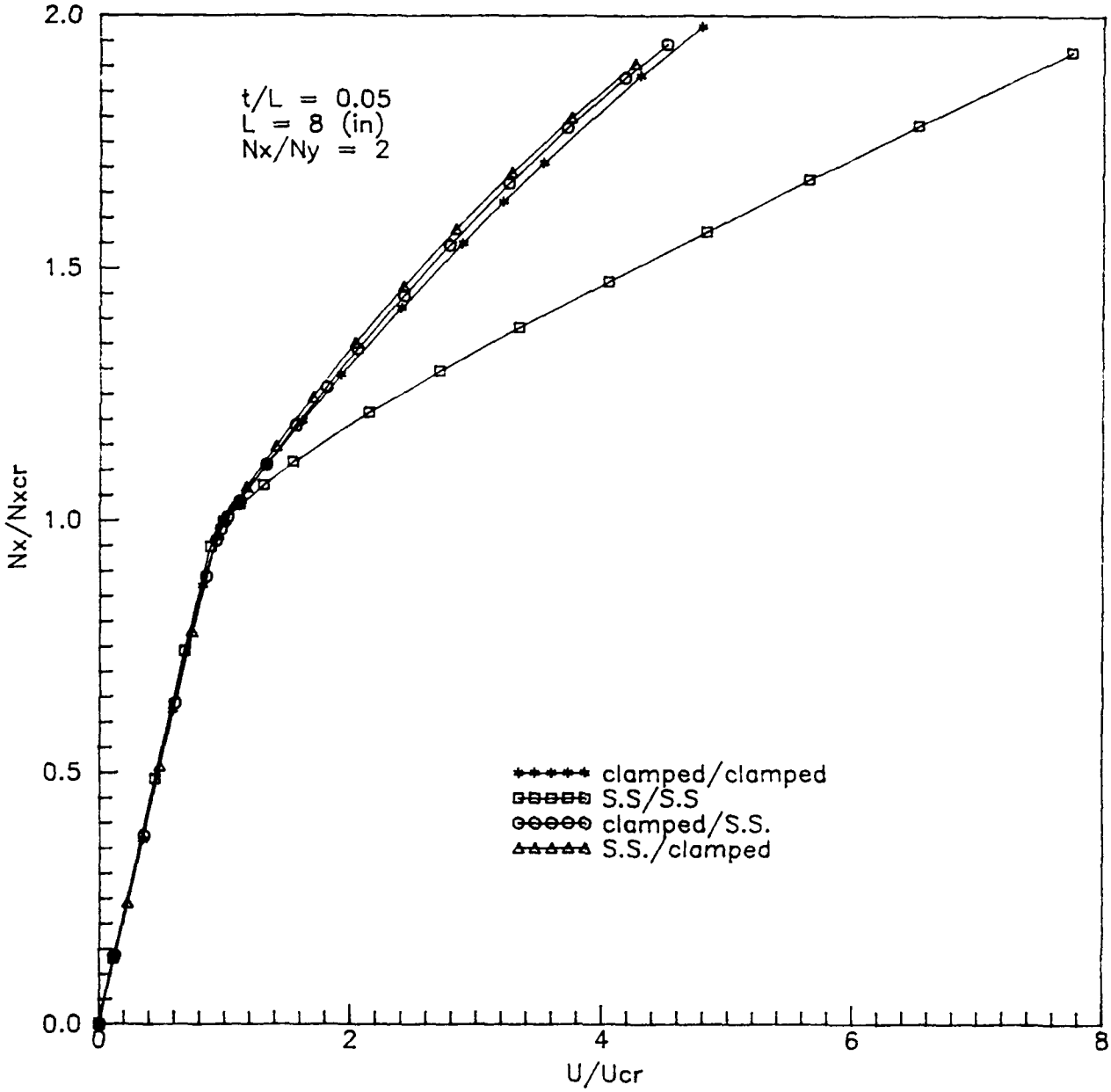

Fig. 24. Effect of boundary conditions on buckling and postbuckling response of a unidirectional laminate plate under biaxial compression ($N_x/N_y = 2$, $t/L = 0.05$)

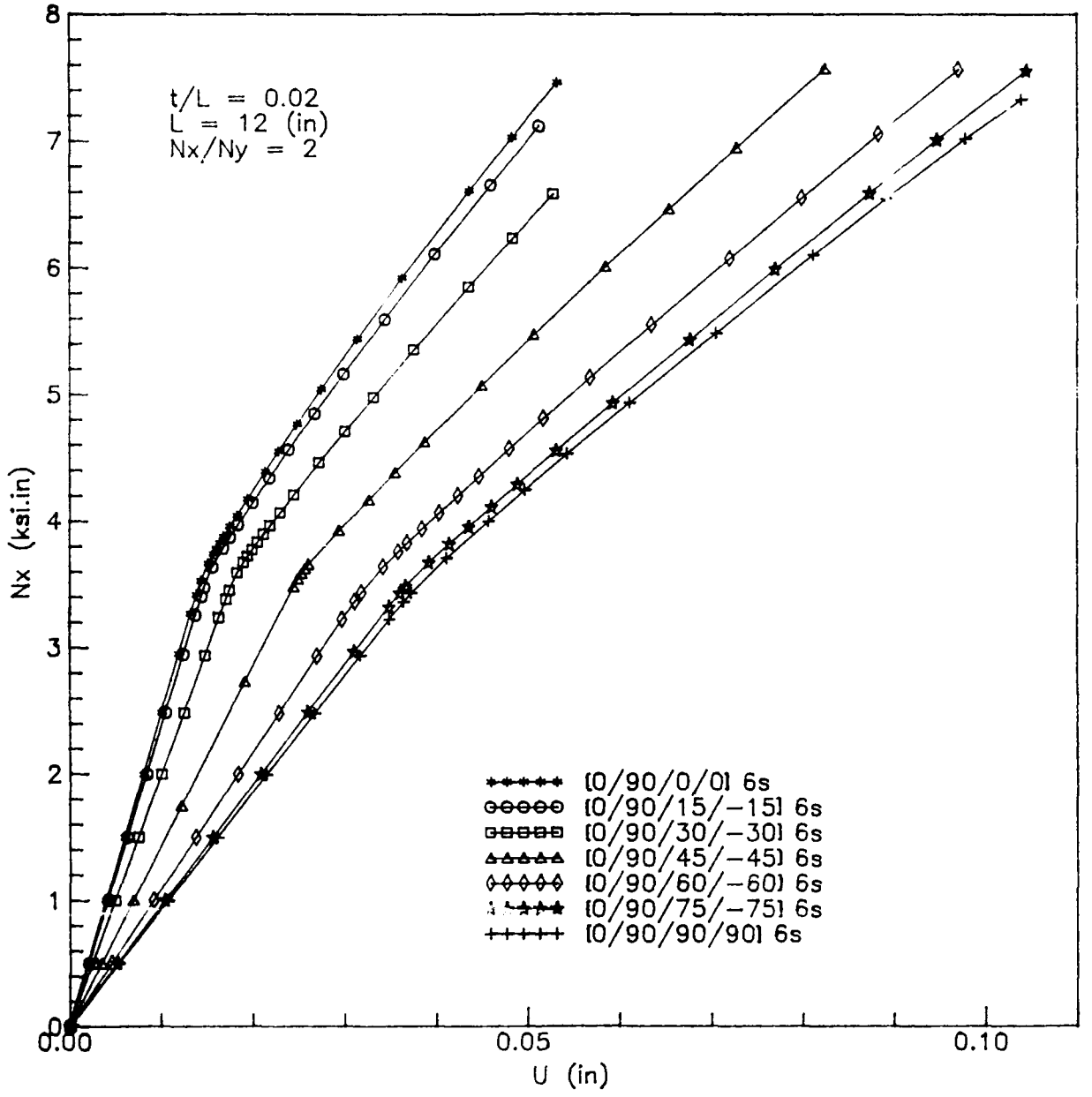

Fig. 25. Effect of lamination layup on buckling and postbuckling response of clamped plates under biaxial compression ($N_x/N_y = 2$, $t/L = 0.02$)

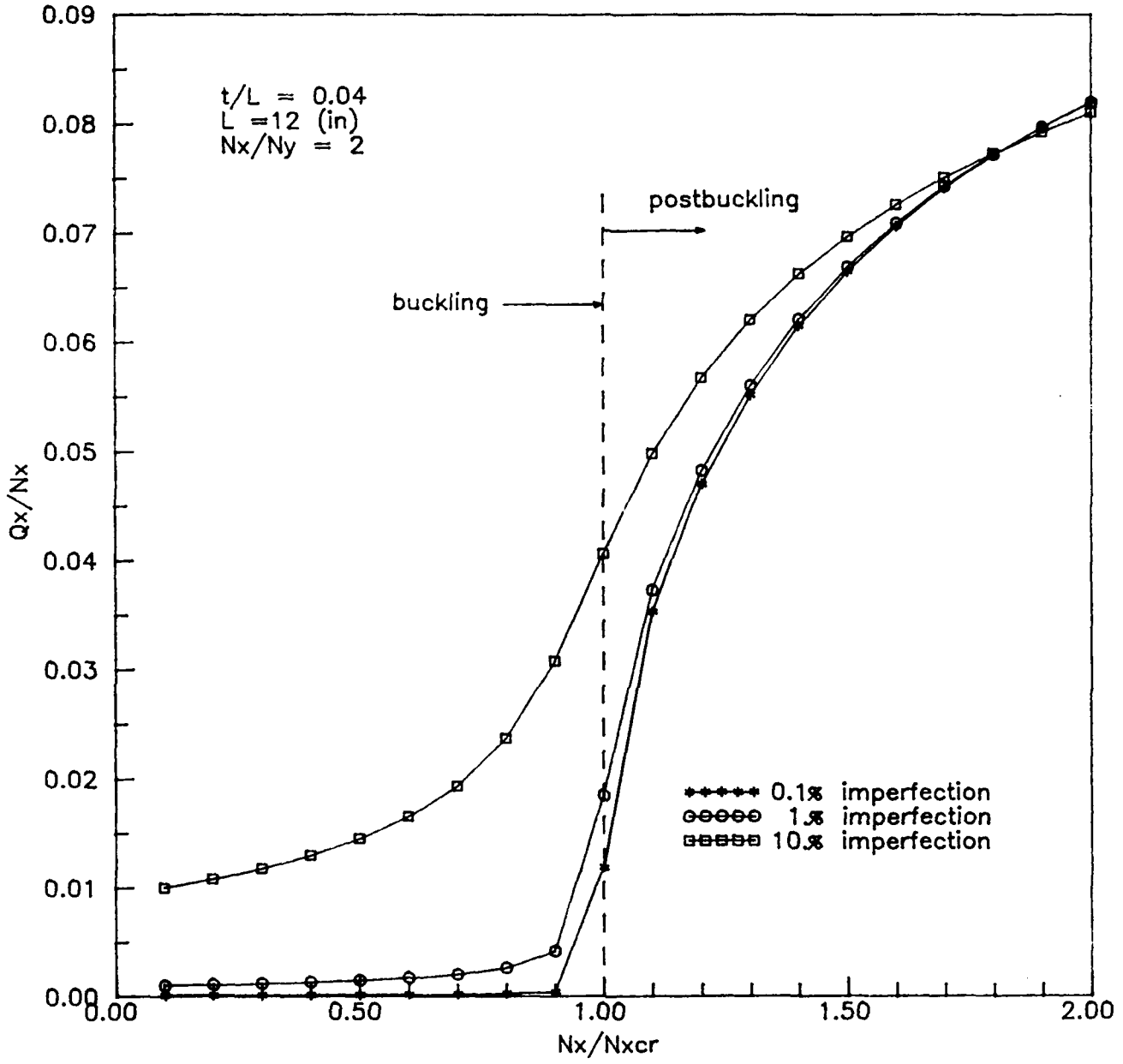

Fig. 26. Effect of imperfection sensitivity on transverse shear Q_x at (-3,-3) (in) in a clamped $[0/90/\pm45]_{12s}$ plate under biaxial compression ($N_x/N_y = 2$, $t/L = 0.04$)

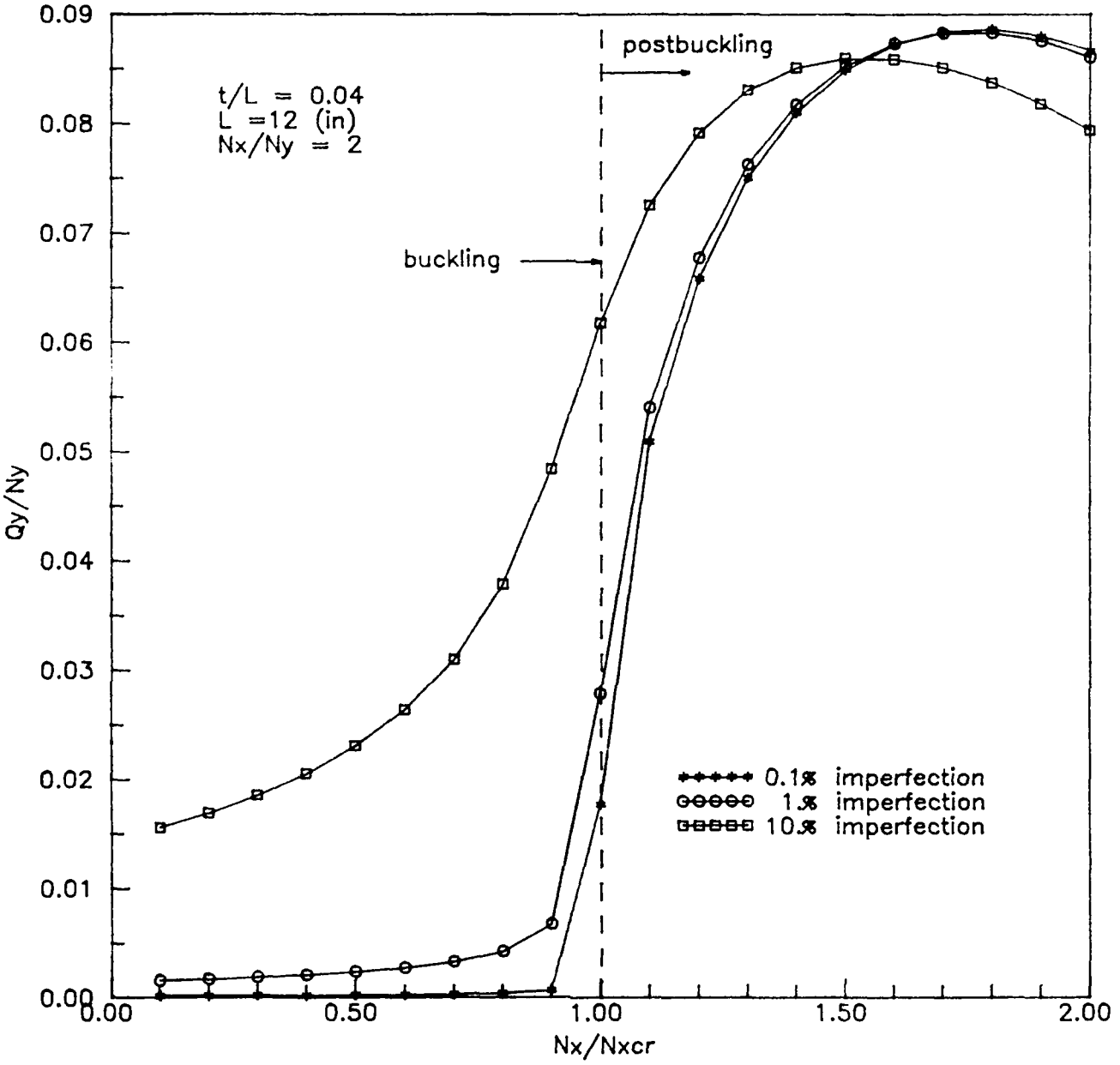

Fig. 27. Effect of imperfection sensitivity on transverse shear Q_y at (-3,-3) (in) in a clamped $[0/90/\pm45]_{12s}$ plate under biaxial compression (N_x/N_y = 2, t/L = 0.04)

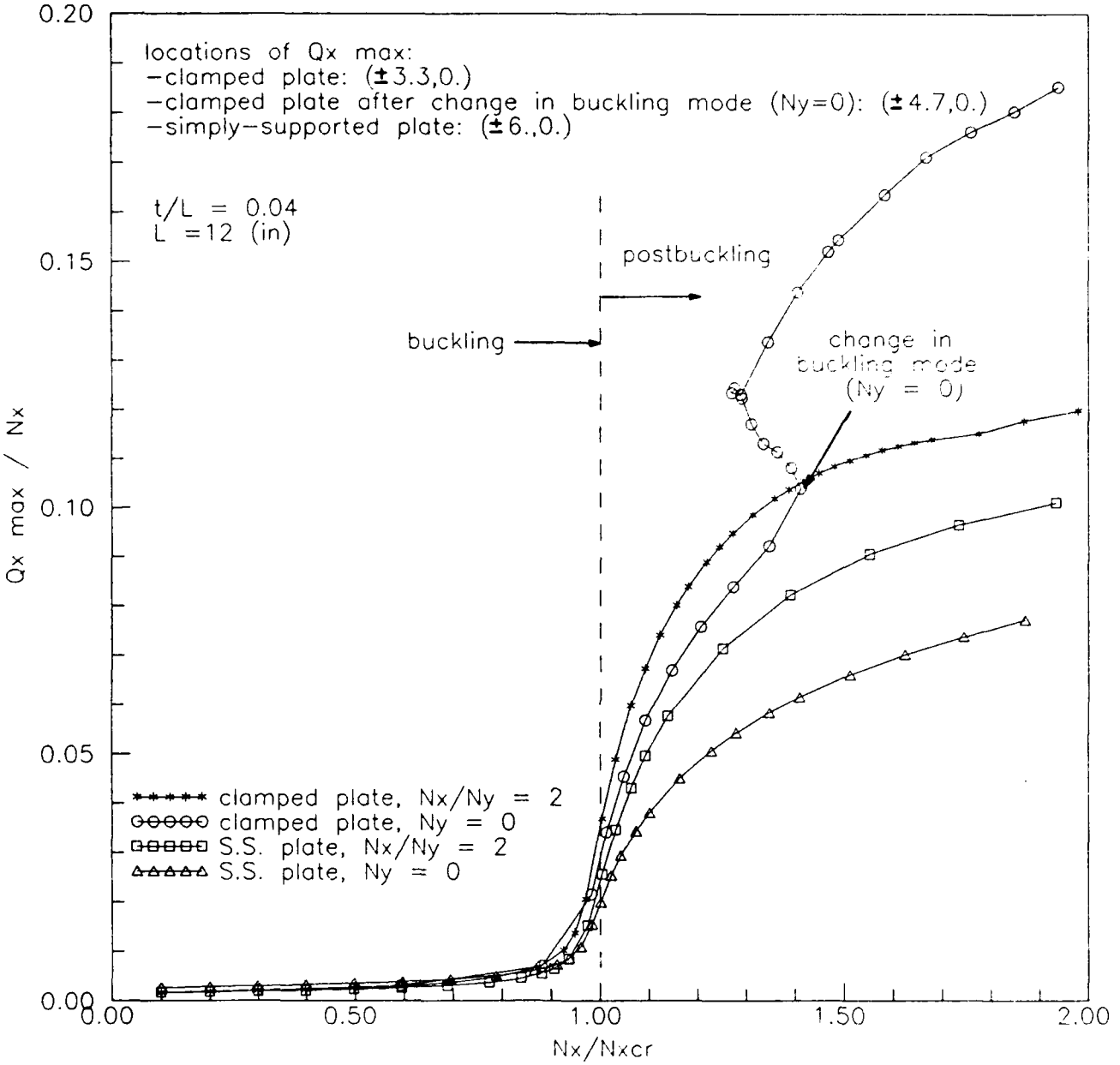

Fig. 28. Effects of boundary conditions and stress-biaxiality on maximum transverse shear Q_x in a $[0/90/\pm45]_{12s}$ laminate (t/L = 0.04)

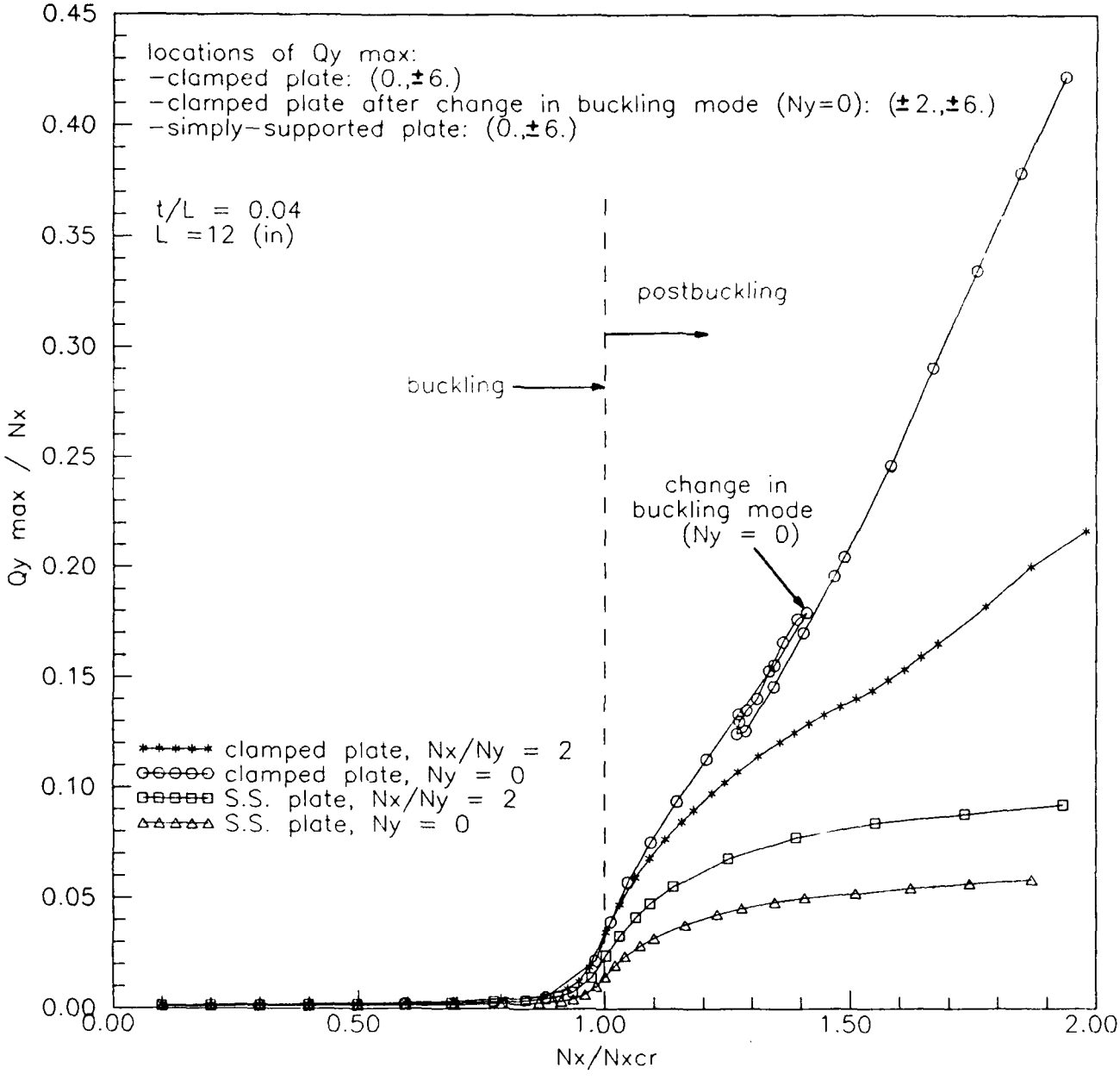

Fig. 29. Effects of boundary conditions and stress-biaxiality on maximum transverse shear Q_y in a $[0/90/\pm45]_{12s}$ laminate (t/L = 0.04)

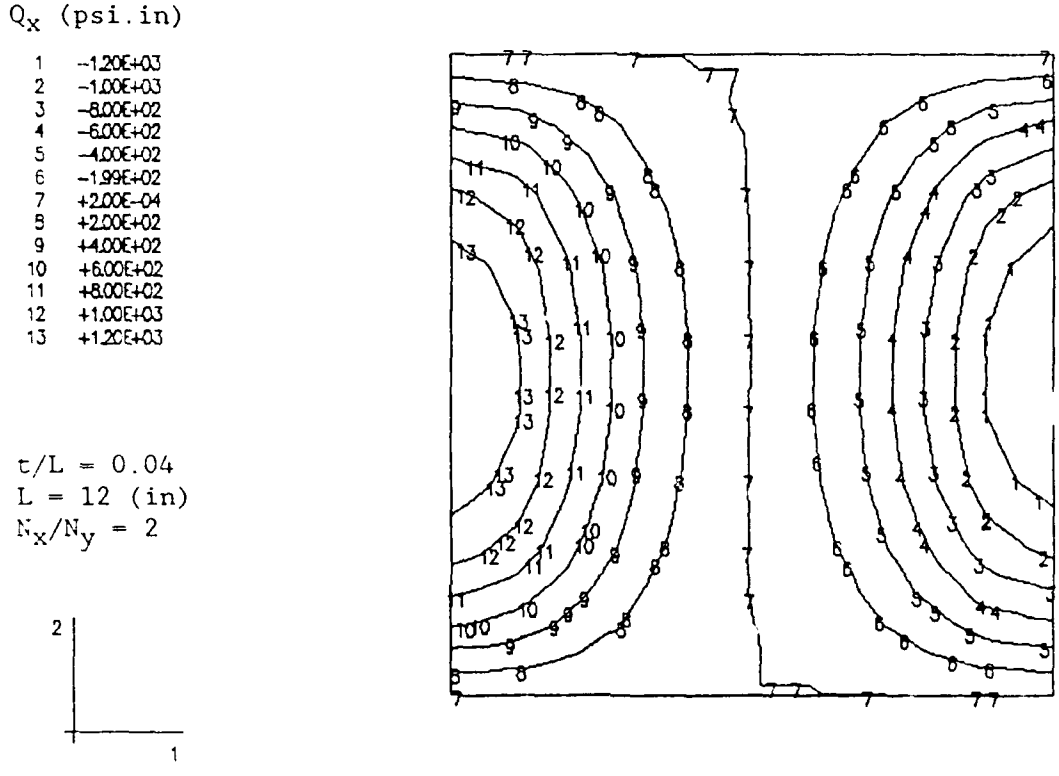

Fig. 30. Distribution of transverse shear Q_x at $N_x = 1.5\ N_{xcr}$ in a simply-supported $[0/90/\pm45]_{12s}$ plate under biaxial compression ($N_x/N_y = 2$, $t/L = 0.04$)

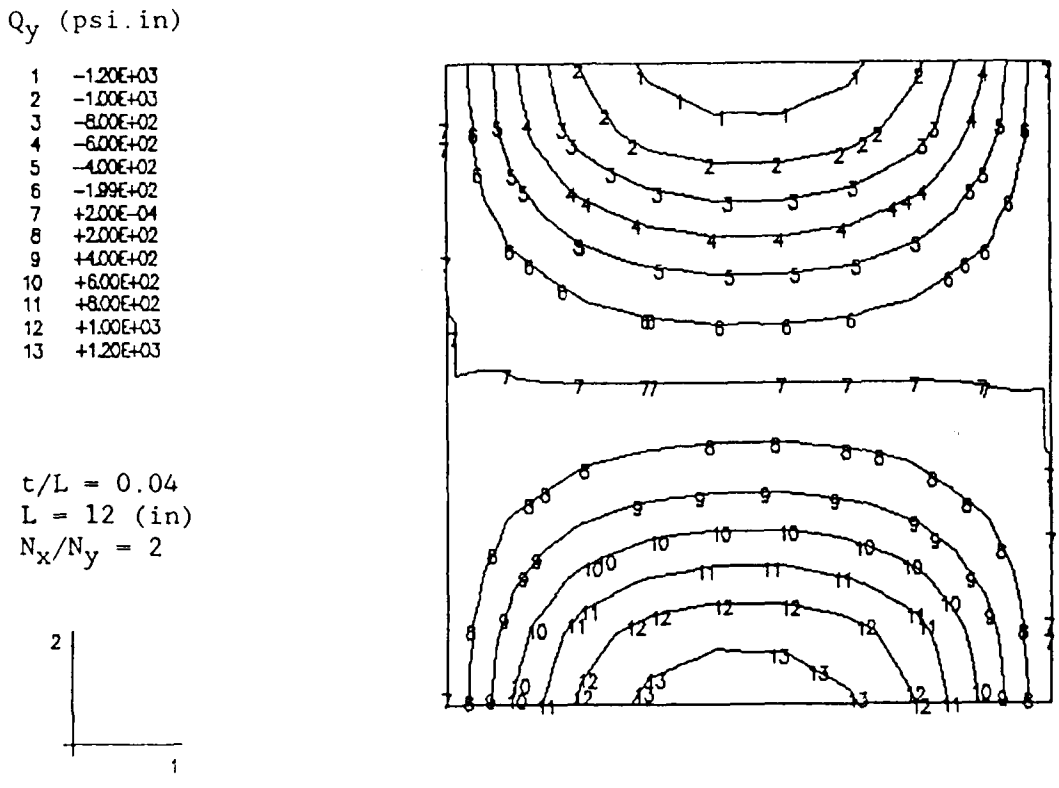

Fig. 31. Distribution of transverse shear Q_y at $N_x = 1.5\ N_{xcr}$ in a simply-supported $[0/90/\pm45]_{12s}$ plate under biaxial compression ($N_x/N_y = 2$, $t/L = 0.04$)

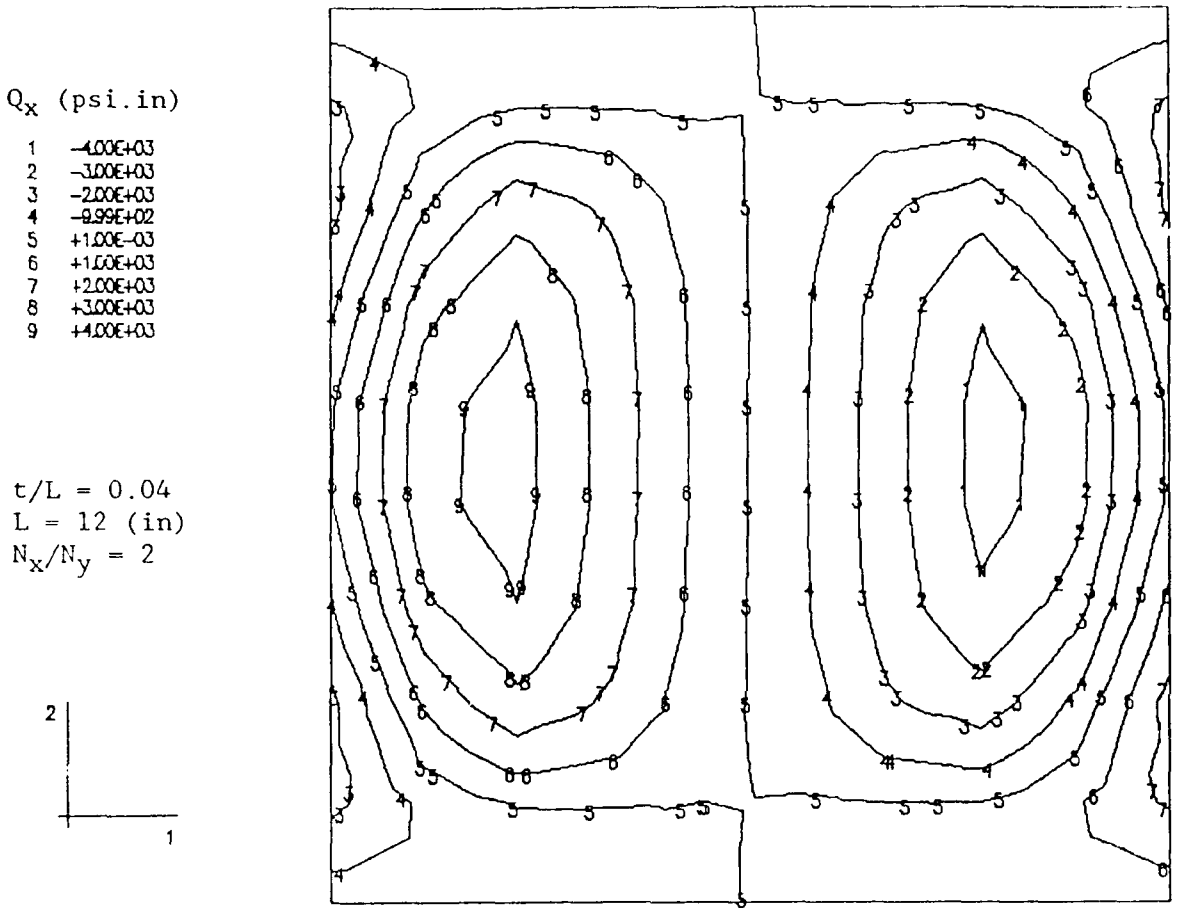

Fig. 32. Distribution of transverse shear Q_x at $N_x = 1.5\ N_{xcr}$ in a clamped $[0/90/\pm45]_{12s}$ plate under biaxial compression ($N_x/N_y = 2$, $t/L = 0.04$)

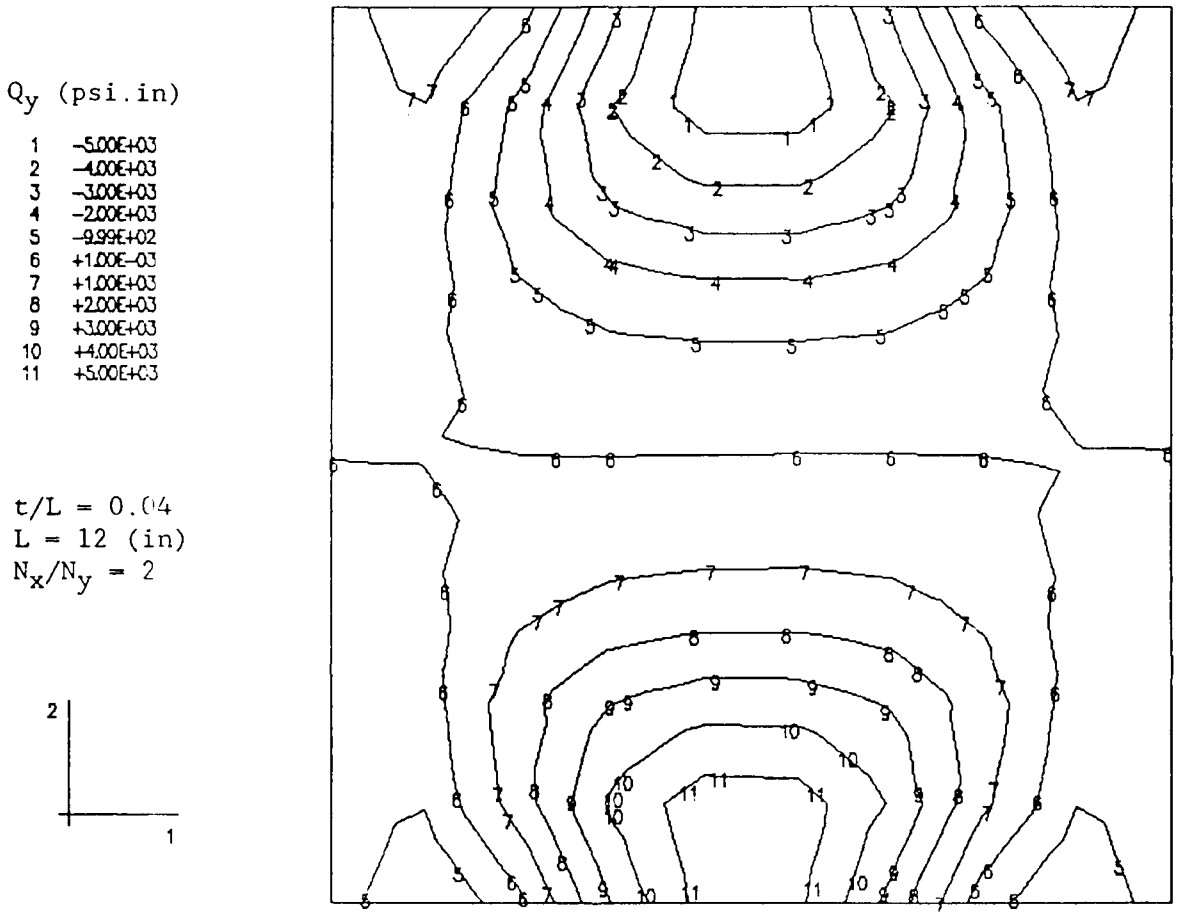

Fig. 33. Distribution of transverse shear Q_y at $N_x = 1.5\ N_{xcr}$ in a clamped $[0/90/\pm45]_{12s}$ plate under biaxial compression ($N_x/N_y = 2$, $t/L = 0.04$)

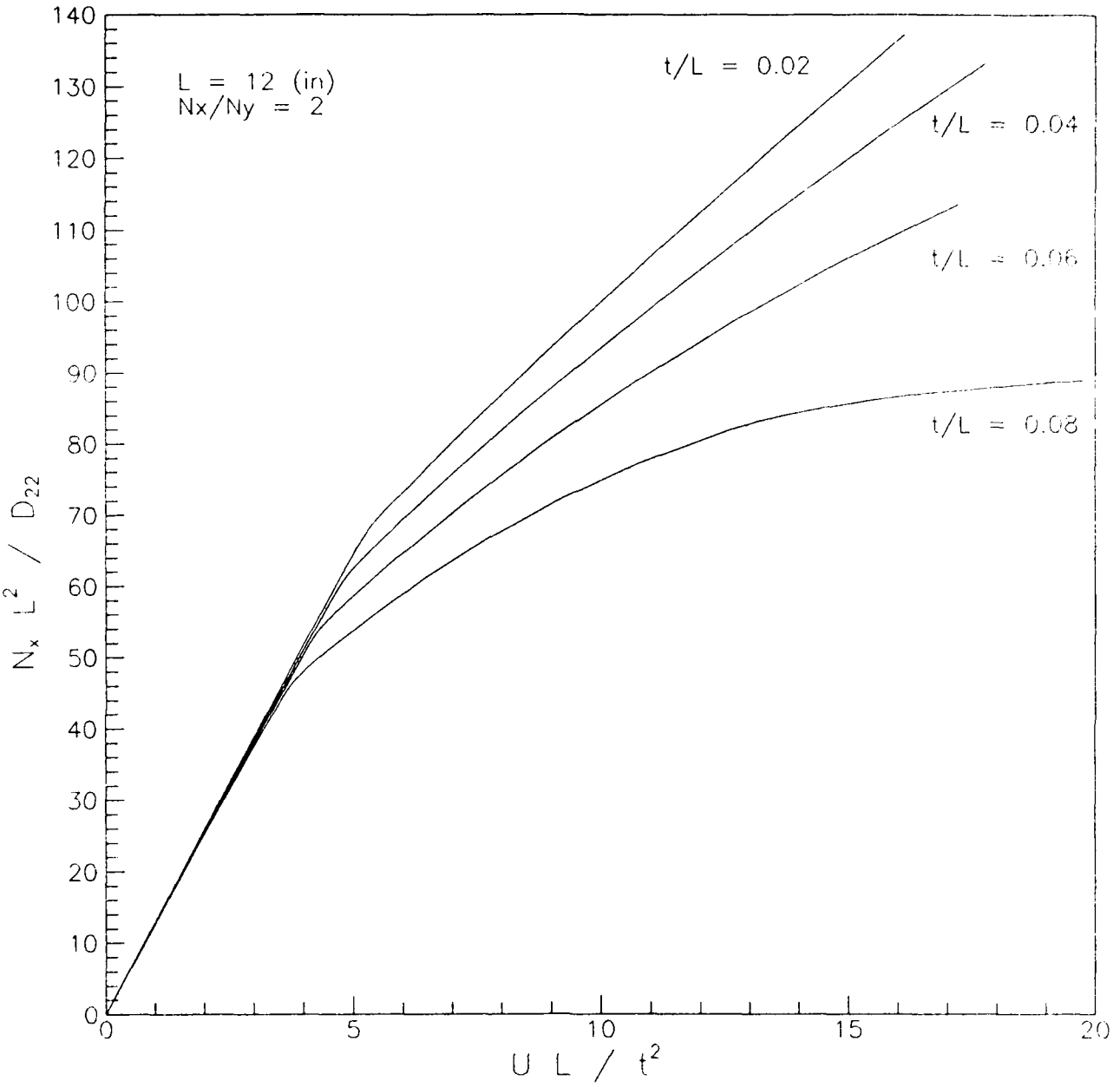

Fig. 34. Effect of laminate thickness on buckling and postbuckling response of a clamped $[0/90/\pm45]_{ns}$ plate under biaxial compression ($N_x/N_y = 2$)

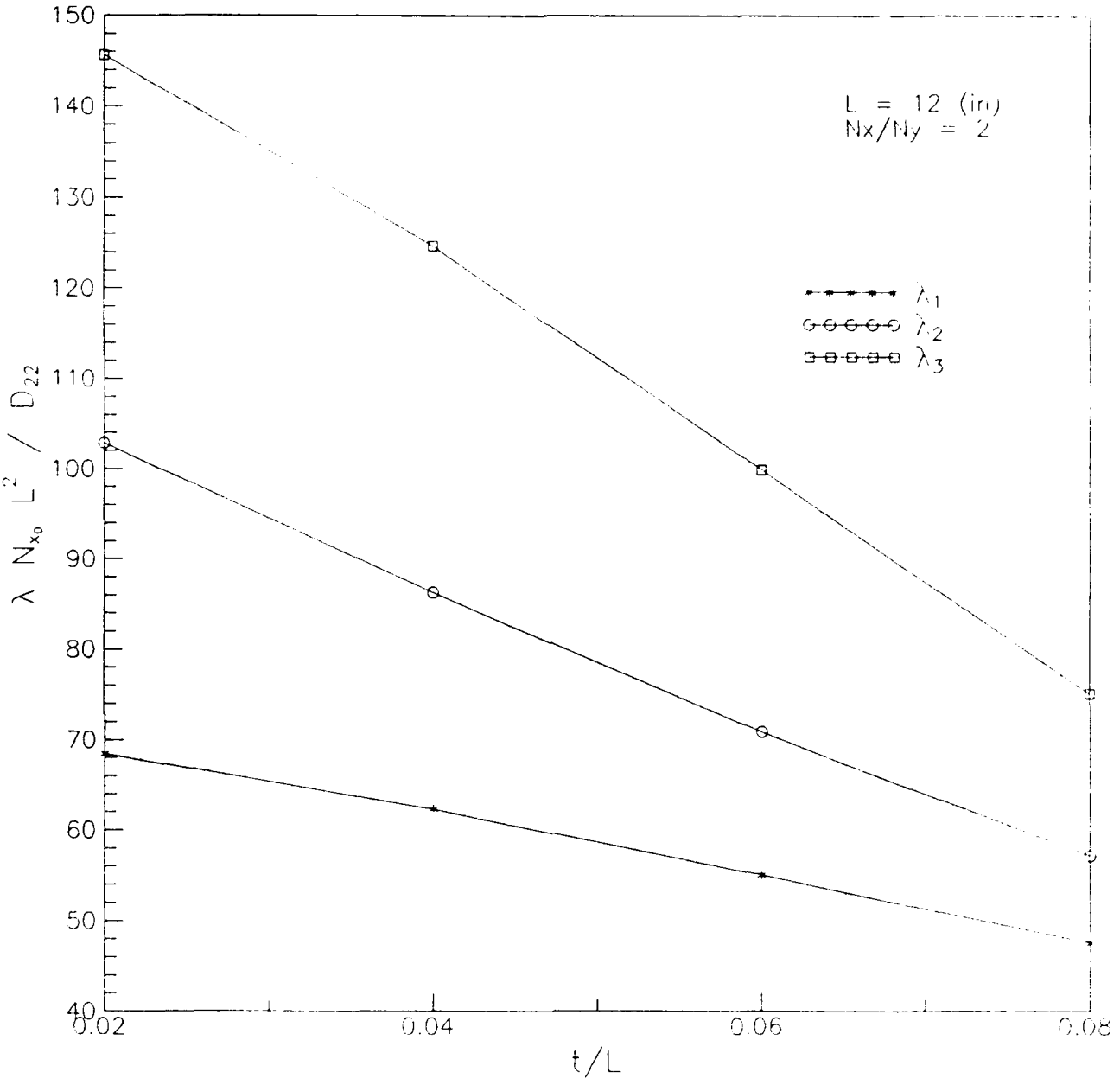

Fig. 35. Effect of laminate thickness on lowest three eigenvalues of a clamped $[0/90/\pm45]_{ns}$ plate under biaxial compression (N_x/N_y = 2)

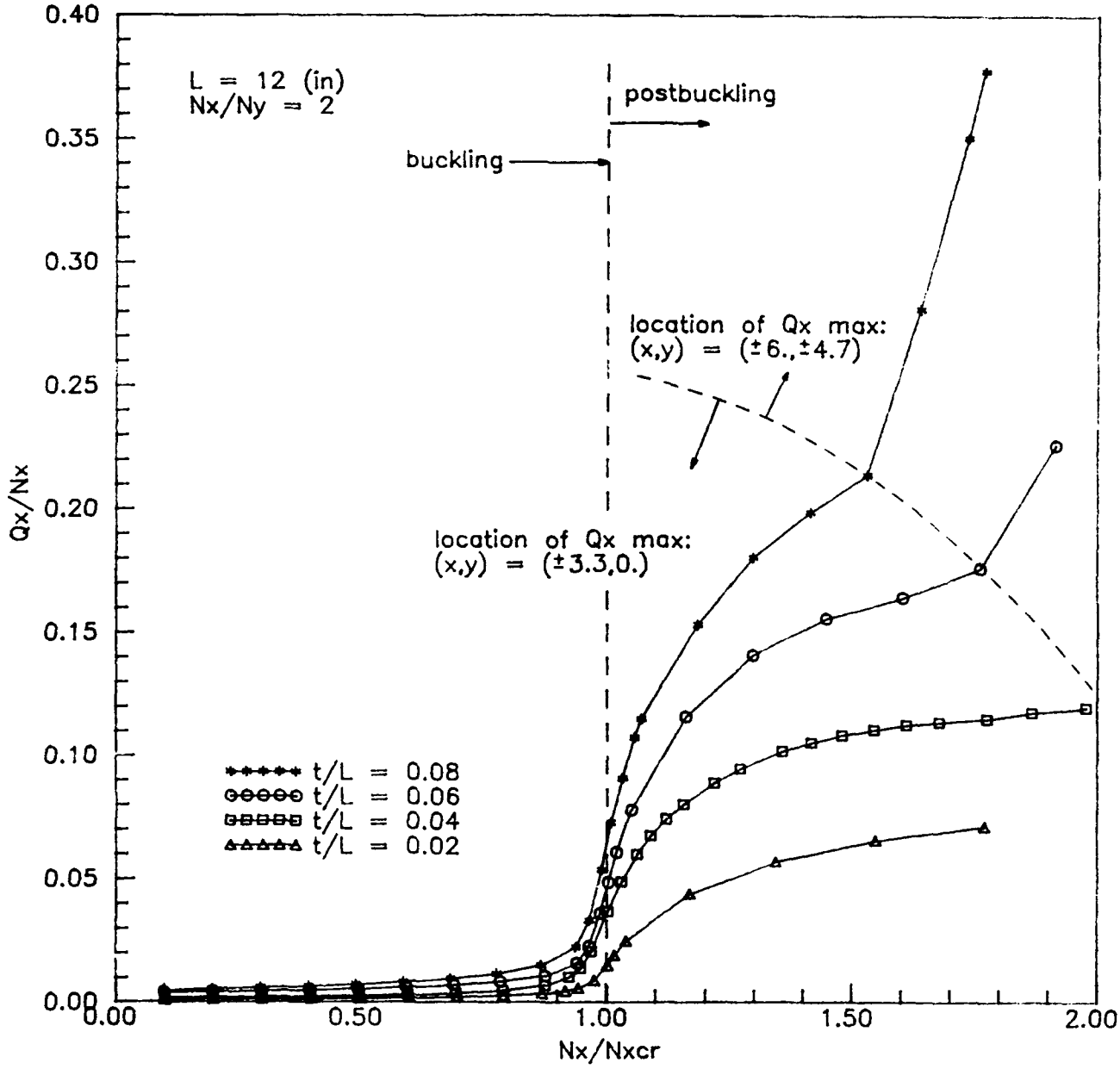

Fig. 36. Effect of laminate thickness on maximum transverse shear Q_x in buckling and postbuckling response of a clamped $[0/90/\pm45]_{ns}$ plate under biaxial compression ($N_x/N_y = 2$)

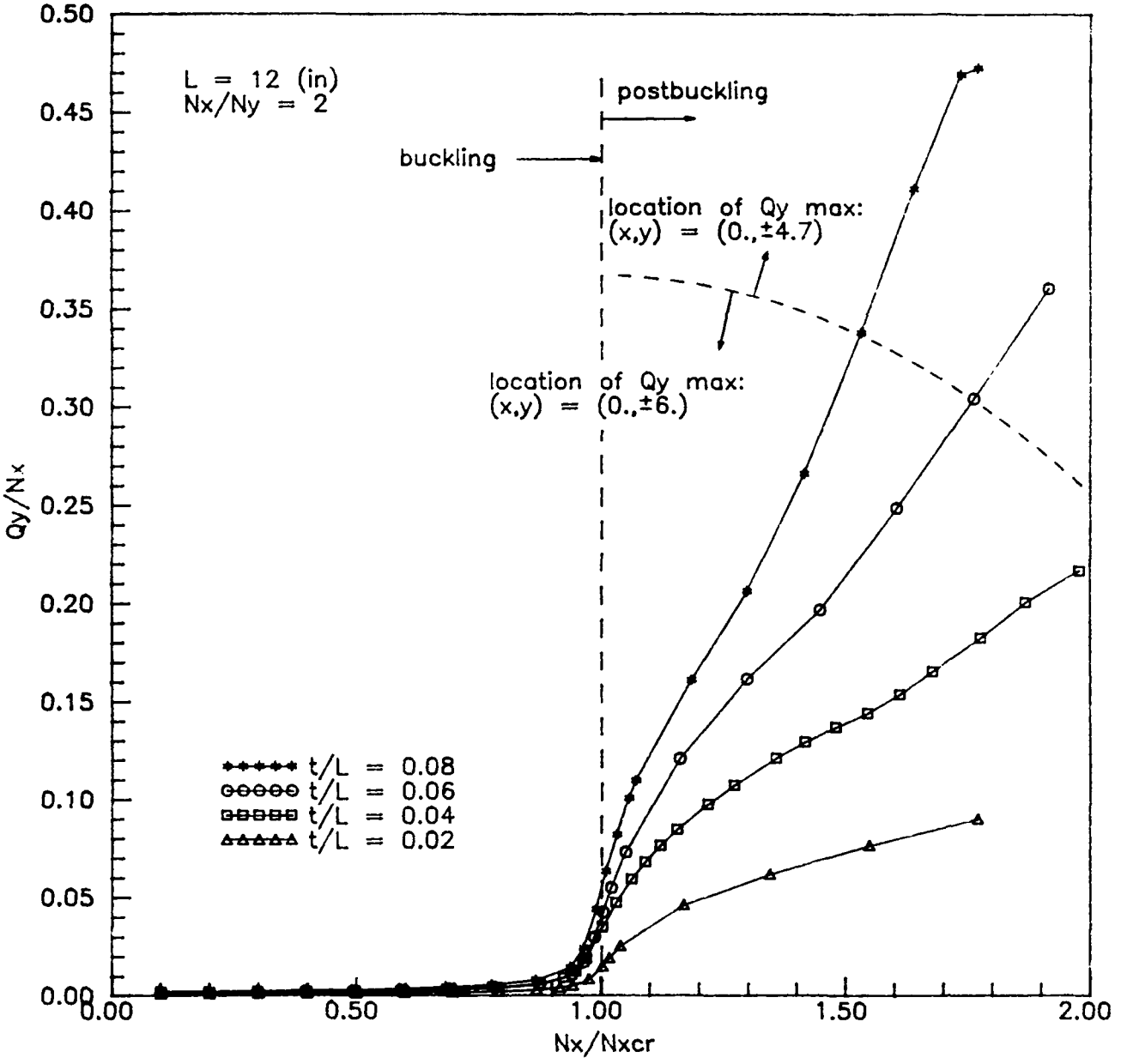

Fig. 37. Effect of laminate thickness on maximum transverse shear Q_y in buckling and postbuckling response of a clamped $[0/90/\pm45]_{ns}$ plate under biaxial compression ($N_x/N_y = 2$)